Felbermayr, Gabriel; Gröschl, Jasmin; Sanders, Mark; Schippers, Vincent; Steinwachs, Thomas

Conference Paper

Shedding Light on the Spatial Diffusion of Disasters

Beiträge zur Jahrestagung des Vereins für Socialpolitik 2018: Digitale Wirtschaft - Session: Economic Geography, No. E10-V1

Provided in Cooperation with:
Verein für Socialpolitik / German Economic Association

Suggested Citation: Felbermayr, Gabriel; Gröschl, Jasmin; Sanders, Mark; Schippers, Vincent; Steinwachs, Thomas (2018) : Shedding Light on the Spatial Diffusion of Disasters, Beiträge zur Jahrestagung des Vereins für Socialpolitik 2018: Digitale Wirtschaft - Session: Economic Geography, No. E10-V1, ZBW - Leibniz-Informationszentrum Wirtschaft, Kiel, Hamburg

This Version is available at:
https://hdl.handle.net/10419/181556

CESifo WORKING PAPERS

7146
2018

July 2018

Shedding Light on the Spatial Diffusion of Disasters

Gabriel Felbermayr, Jasmin Gröschl, Mark Sanders, Vincent Schippers, Thomas Steinwachs

CESifo

Impressum:

CESifo Working Papers
ISSN 2364-1428 (electronic version)
Publisher and distributor: Munich Society for the Promotion of Economic Research - CESifo GmbH
The international platform of Ludwigs-Maximilians University's Center for Economic Studies and the ifo Institute
Poschingerstr. 5, 81679 Munich, Germany
Telephone +49 (0)89 2180-2740, Telefax +49 (0)89 2180-17845, email office@cesifo.de
Editors: Clemens Fuest, Oliver Falck, Jasmin Gröschl
www.cesifo-group.org/wp

An electronic version of the paper may be downloaded
· from the SSRN website: www.SSRN.com
· from the RePEc website: www.RePEc.org
· from the CESifo website: www.CESifo-group.org/wp

CESifo *Working Paper No. 7146*
Category 10: Energy and Climate Economics

Shedding Light on the Spatial Diffusion of Disasters

Abstract

Climate research suggests that global warming will lead to more frequent and more extreme natural disasters. Most disasters are local events with effects on local economic activity. Hence, assessing their economic impacts with the help of econometric country-level analysis may lead to biased results. Moreover, correct identification is further complicated by the possibility that local shocks shift production and consumption to neighboring locations. In this paper, annual night-time light emission data covering about 24,000 grid cells for the years 1992-2013 are matched to geocoded information on meteorological and geological events. Spatial econometric panel methods are applied to account for interdependencies between locations. Interpreting variation in light emissions as reflecting changes in economic activity, findings convey evidence for pronounced local average treatment effects and strong spatial spillovers, particularly for weather shocks. Moreover, substantial heterogeneity across income groups and regions is identified.

JEL-Codes: F150, O180, O440, Q540, R120.

Keywords: natural disaster and weather shocks, night-time light emission, spatial spillovers, grid cell analysis.

Gabriel Felbermayr
Ifo Institute – Leibniz Institute for Economic Research at the University of Munich / Germany
felbermayr@ifo.de

Jasmin Gröschl
Ifo Institute – Leibniz Institute for Economic Research at the University of Munich / Germany
groeschl@ifo.de

Mark Sanders
Utrecht School of Economics / The Netherlands
m.w.j.l.sanders@uu.nl

Vincent Schippers
Utrecht School of Economics
Utrecht / The Netherlands
v.g.schippers@uu.nl

Thomas Steinwachs
Ifo Institute – Leibniz Institute for Economic Research at the University of Munich / Germany
steinwachs@ifo.de

July 5, 2018
The authors thank Ilan Noy, Wouter Botzen, participants at FIW Workshop on International Economic Networks Vienna, Development Economics and Policy Conference Zurich, IOSE St. Petersburg, EGIT Düsseldorf, ETSG Florence, IO and Trade Seminar at LMU Munich, Seminar at Victoria University Wellington, Workshop on Geodata and Economics Braunschweig, Conference on Environmental Economics in Orléon for useful comments and suggestions. Jasmin Gröschl gratefully acknowledges funding from the German Research Foundation (DFG) under project GR4896/1-1. Thomas Steinwachs gratefully acknowledges funding from the Leibniz Association under project SAW-2016-PIK-1. All remaining errors are our own.

1. Introduction

A large body of research suggests that global warming is a reality and that it will result in more frequent and more extreme natural disasters; see IPCC (2014) for a synthesis report. Hence, it is important to improve the understanding of the economic consequences of natural disasters around the globe. This paper provides an attempt at measuring the average impact on local economic activity of various types of meteorological and geological events and their spatial spillovers.

While the direct material destruction and the toll on human lives caused by disasters are all too evident, measuring their economic consequences is prone to difficulties. Early papers have investigated the relation between direct disaster damages, deaths, and economic development (see e.g. Kahn, 2005; Anbarci et al., 2005). Building on these, a growing literature predominantly uses aggregated cross-country data to investigate the effect of natural disasters on economic growth.[1] Findings depend heavily on the type of disaster data, country sample, and the types of disasters studied (Raddatz, 2007; Cavallo et al., 2013; Felbermayr and Gröschl, 2014).

Several data and specification issues explain the ambiguity of findings. First, many studies use information on the incidence of natural disasters from databases drawn from insurance records or news.[2] This introduces severe reporting, selection and endogeneity biases, as both insurance penetration and damage caused are correlated with development (Felbermayr and Gröschl, 2014). In addition, such data lack information on physical intensities of events that have not caused sufficient damage to qualify as a disaster (Strömberg, 2007). To tackle these issues, Felbermayr and Gröschl (2014) proposed and collected a database with information on the exogenous physical intensities of geological and meteorological events from primary sources at the country-level.[3] Their evidence clearly suggests a negative impact, with a substantial growth penalty for the worst 5% of shocks.

Most papers conduct their analysis at the country level. However, mapping natural events to countries of heterogeneous size can result in measurement error and attenuation bias (Noy, 2009). By aggregating local events data to the country level, important information is lost. First, similar events causing similar damage and impact on income show up as a major shock in a small island state's gross domestic product (GDP), whereas they might go unnoticed in a large country.[4] Second, the difference between an event striking a

[1] For comprehensive literature reviews, see Cavallo et al. (2011) and Klomp and Valckx (2014).

[2] For example, this is the case for the often used data base provided by Munich-Re (EM-DAT), the world's largest reinsurance firm.

[3] https://www.cesifo-group.de/ifoHome/facts/EBDC/Ifo-Research-Data/Ifo_GAME_Dataset.html.

[4] For example, Strobl (2011) illustrates that, in the United States, hurricane effects wash out at the

densely populated coastal region or an empty desert is lost, particularly in countries with a large territory. Third, in large economies, geographic spillover effects may disguise the full local treatment effect. Hence, regressing country level GDP (growth) on aggregate indicators of local natural events might yield biased estimates.

The challenge is to find a proxy of local economic activity at the same level of geographical detail as the meteorological and geological data.[5] Satellite technology has produced numerous data products that contain information on human presence and activity at a very fine level of spatial resolution. Recent papers have started to explore these data; for a survey see Donaldson and Storeygard (2016). Night-time light emissions have been shown to strongly correlate with economic activity (cp., Henderson et al., 2012; Nordhaus and Chen, 2015; Pinkovskiy and Sala-i Martin, 2016). While Henderson et al. (2012) investigate the informational value of night-lights in estimating economic growth at the country level, an emerging literature investigates even smaller sub-national units: Michalopoulos and Papaioannou (2013, 2014) focus on ethnic homelands, Hodler and Raschky (2014) on sub-national administrative units, Storeygard (2016) on cities, Henderson et al. (2017) on uniform grid cells and Bleakley and Lin (2012) on locations along rivers as natural features. The broad consensus is that growth in remotely sensed night-time light provides a very useful proxy for GDP growth over the long-run but also accurately tracks short-run fluctuations in economic growth.

Using night-lights as a proxy for economic activity has at least three benefits for this research: First, while growth in lights reflects growth in economic activity, measurement error in night-lights is not correlated with the level of income per capita.[6] Second, night-light information is available for all countries at a standard geographic resolution.[7] Third, GDP per capita statistics fail to account for an often sizable informal economy.[8] In

state level and even more so at the national level, leaving no trace in economic growth rates.

[5]While industrialized countries record income and production for sub-national administrative units, the same data is scarce for most other countries. The G-Econ project provides gross product per capita data at a $1^\circ \times 1^\circ$ cell level. It uses gross product data for the lowest available political subdivision. For most low-income countries, this unit remains the national level, such that regional income estimates are largely driven by (an often estimated) population distribution. This methodology leaves serious GDP measurement problems unaddressed for a substantial part of the globe. As discussed by Henderson et al. (2012), national accounts are particularly weak in low-income countries.

[6]This is especially relevant for studying economic impacts in developing countries, where measurement error on the official GDP statistics is large. Henderson et al. (2012) use night-lights to find improved measures of income growth statistics for countries with low quality national accounts.

[7]Thus a number of low-income countries can be included that provide no national account GDP statistics (i.e., Myanmar or Somalia), while these countries frequently do experience extreme natural events. This avoids selection bias stemming from samples limited by availability of national accounts for GDP statistics.

[8]See, e.g., Schneider and Enste (2000); Schneider (2005) for worldwide estimates on the informal economy and Tanaka and Keola (2017) for a study using night lights data to identify the informal sector.

addition, natural disasters tend to affect the poorest members of society, who are often active in the informal economy and whose activity is hard to measure (for an excellent discussion, see World Bank and United Nations, 2010). Yet, being able to capture (part of) the informal sector is important to identify the true effect of natural extreme events.

This study is not the first one using night-lights to assess disaster impacts at the local level. Bertinelli and Strobl (2013) and Elliott et al. (2015) study direct hurricane and typhoon impacts on light emission. They find reduced local light growth caused by hurricanes in the Caribbean and typhoons in coastal China, respectively, where the size of the effect found is twice as large compared to using GDP data at the country level. Although both papers are limited in regional focus and evaluate the impact of a specific disaster type, their findings strengthen the case for assessing disaster impacts at the local level and and propose night-light emissions as a suitable proxy. In this paper, the empirical analysis is extended to 24,000 geographical units of $0.5^{\circ}\times0.5^{\circ}$ in 197 countries over 22 years and a wide array of different natural events is studied.

Zooming in on the grid cell level risks violating the standard assumption that errors are uncorrelated across units of observation. Especially weather shocks have a spatial extent, often affecting multiple locations at once. Even though there is variation across these locations, exogenous treatment is potentially spatially correlated. If spatial spillover effects exist between neighboring locations, the treatment of neighbors may have explanatory power, such that not explicitly modeling the spatial relationship gives rise to correlated errors and causes omitted variable bias. Another issue arises if exogenous shocks had a spatial correlation structure which is imperfectly captured by the disaster data. While some measurement error is certainly present, there is no evidence for a systematic spatial pattern. However, there may still be other omitted variables such as trade or migration between cells which imply that errors may be spatially correlated even if the treatment of neighbors is controlled for and the intensity of natural disasters has no systematic measurement error. Hence, the grid cell approach requires an explicit modeling of spatial treatment spillovers and of spatial autocorrelation in the residuals. The direction of these spatial spillovers depends, amongst other things, on specialization patterns: if a neighboring region specializes in similar industries, economic activity may shift towards it. If a neighboring region specializes in down-stream or up-stream industries, it may well be hurt by the shock. Hence, the relationship between the two regions may be governed by complementarity or by substitution effects.[9] This paper does not explore the exact mechanisms through which such spillovers arise, but makes a first attempt to empirically

[9]This logic is well known from the international trade literature, see Hsieh and Ossa (2016) for a recent application.

measure them.

In sum, this paper takes the analysis of economic impacts of natural disasters to global uniform grid cell data and evaluates the local economic effects of natural shocks. For this, a large data set of geological and meteorological events (ifo GAME Database) is updated and matched with available data on night-time light emissions as a proxy for economic activity. Following Costinot et al. (2016), the globe is partitioned into fields along latitude and longitude. Along with economic variables, various disaster types (storms, extreme precipitation, droughts, cold waves, and earthquakes) are mapped to specific grid cells using geographical information systems. In this paper, a balanced panel of 24,184 grid cells is created with a resolution of $0.5^\circ \times 0.5^\circ$ (approximately 55×55 km at the equator) spread across 197 countries from 1992 to 2013. Using spatial econometric panel techniques, the impact of various types of events on the growth of night-time light emissions is estimated, controlling for cell population, a set of year- and cell fixed effects and accounting for spatial autocorrelation in the error term.

Main results show a reduction in night-time lights after storms, cold waves and extreme precipitation events. For these types of events, there is strong evidence for positive spatial spillover effects within an 80 km radius. At the mean, effects are moderate and range in the order of 0.1-0.3 percentage points. At the extremes of our disaster measures, effects are pronounced and amount to several percentage points reduction in light growth in the short run. More specifically, evaluated at the average estimated lights-to-GDP growth elasticity, a one standard deviation increase in wind speeds leads to a reduction in income growth of 0.33 percentage points. With a time lag, the local effect is four times as large and spillovers from *one* cell increase local lights growth by 0.08 percentage points, corresponding to an income growth spillover of 0.13 percentage points for a one standard deviation increase in wind. Similarly, a one standard deviation increase in excessive precipitation and cold waves decrease income growth by 0.17 and 0.25 percentage points, respectively. With a time lag, excessive precipitation *increases* income growth by 0.12 percentage points, while the effect of cold spells persists to be negative by 0.11 percentage points. Associated contemporaneous spillovers amount to 0.03 and 0.07 percentage points, respectively. As droughts mostly affect agricultural outcomes, they do not seem to be associated with light emissions. Short-run negative spatial spillovers of these events are largely driven by rural rather than urban cells, suggesting that droughts cause indirect damages in rural economies. Results are robust to top- and bottom-coding, increasing the spatial radius, the temporal aggregation method and controlling for time-varying country characteristics or the use of a global spillover specification. There is evidence for heterogeneity across

income groups and world regions. Overall, results are mainly driven by cells in low- and middle-income economies.

The remainder of the paper is organized as follows: Section 3 describes the econometric methodology. In section 2, data sources and the construction of the data set are discussed. Section 4 presents baseline results and shows the existence of both local treatment effects as well as spillovers to neighboring cells. Results are tested with respect to a number of measurement and specification variations. Finally, the assessment zooms in on the heterogeneity of effects across income groups and world regions. The last section concludes.

2. Measuring Economic Activity and Natural Disasters at the Cell Level

2.1. Light Emissions

First, the dependent variable, growth in night-time light emissions, which is taken as a proxy for local economic activity, is described. The data stem from the US Air Force Defence Meteorological Satellite Program (DMSP). They comprise yearly composite satellite images from which the yearly mean luminosity of each pixel can be extracted as a digital number (DN).[10] To align the data with the overall setup, all lights pixels that do not cover land surface are excluded[11] and the literature is followed by masking all pixels within gas flaring zones identified by Elvidge et al. (2009).[12] Similarly, areas around volcanoes are masked.[13]

In addition, years in which more than one composite night-light image is available are dealt with. As the on-board sensors degrade over time, the DMSP launches a new

[10] Appendix A.1 provides supplementary information on data generation and graphical illustration.

[11] Even though substantial presence of light at sea exists (e.g., fishing boats or oil rigs), this economic activity cannot directly be attributed to any location on land and is therefore excluded. Further, natural disasters affect light emission at sea differently from that on land. At sea, lights may be mobile and seafaring may be ceased temporarily.

[12] The DMSP Operational Linescan System instruments record gas flares (typically resulting from gas disposal at oil production sites) as heavily over-glowing areas that differ markedly from areas with lights of electric origin. This affects approximately 2,300 grid cells; 0.89% of global land area.

[13] Volcanic eruptions show up in light data if they involve prolonged lava flows. If they are short-lived, they are excluded from the annual stable lights products by default. Some volcanoes (e.g., Etna in Italy and Popocatepetl in Mexico), however, show presence of lava flows throughout the entire period observed (1992-2013). Persistent light at all known volcanic locations is approximately circular with a consistent radius of 3 to 5 km. Consequently, these zones are masked from the light data. Two areas with lava flows near to Kilauea (Hawaii) and Nyiranongo (Congo, DRC) are masked manually to account for their spatial size and shape.

satellite every 3 to 6 years. In 12 of the 22 available years, two satellites were in orbit simultaneously. In these cases, the satellite with the best coverage of valid nights per pixel in a given year is selected on the basis of each respective satellite-year layer's summary statistics.[14] If the number of valid nights for a radiance pixel is zero, it is masked from the data. The prepared night-light layers are aggregated to mean light intensity for the $0.5^\circ \times 0.5^\circ$ grid cells.[15]

To translate light changes into economic magnitudes, Henderson et al. (2012) and Storeygard (2016) estimate lights-to-GDP growth elasticities at the country and the Chinese prefecture level, respectively. For both levels of aggregation, they find an elasticity of approximately 0.3. Following their approach allows obtaining an elasticity for the specific sample used in this research: Grid-cell data can be aggregated to the country level using area-weights for the spatial aggregation. Then, the natural logarithm of country level GDP in real currency units is regressed on the log of aggregate night-light intensity and a full set of country and time fixed effects.

Using the full time-span from 1992 to 2013 and the set of 197 countries, estimates suggest an aggregate lights-to-GDP growth elasticity of 0.37. The within R^2 is equal to 0.273, so that time variation in light emissions explains more than a quarter of the variation in GDP within a country over time. Moreover, the country level elasticity of lights to the population density (0.10) is not significantly different from the elasticity of GDP to the population density (0.13).[16] In line with recent literature connecting population density to total factor productivity (TFP) at the grid cell level (Desmet et al., 2018), this finding fosters the adequacy of light emissions as a proxy for gridded economic activity. Figure 1 compares grid cell level lights growth to country level GDP growth over time. Even without adjusting for potential systematic measurement error in the lights data, which will be taken care of econometrically, the plots indicate substantial variation across time and provide suggestive evidence for the co-movement of light and economic

[14] Typically, the lights literature takes the simple average of these images (see, e.g., Chen and Nordhaus, 2011; Henderson et al., 2012; Pinkovskiy and Sala-i Martin, 2016). However, data availability (the number of valid nights that led to pixel construction) can be quite different across satellite-years. This introduces missing observations even if one satellite contains valid information. It also generates potentially spurious mean pixel values in which underlying valid nights enter the final mean with inconsistent weight or may be double-counted. Satellite-year inspection leads to selecting the layer from the respective youngest satellite with only one exception. There is a clear time-trend in the average number of valid nights, which steadily improves as new satellites are launched (see Table A3 in the Appendix).

[15] Additionally the number of top-coded (DN63) and bottom-coded (DN0) pixels in each cell are recorded. For robustness, top- or bottom-coded pixels are excluded in Section 5.1.

[16] One needs to bear in mind that this correlation is obtained by aggregating data to the country-level; this biases the strength of the lights-GDP link downwards. Detailed results are shown in Table A4 in the Appendix. If the regression is restricted to the same time frame as Henderson et al. (2012), the obtained elasticity is 0.35 and the within R^2 is 0.240.

Figure 1: Growth in Lights vs. Growth in GDP

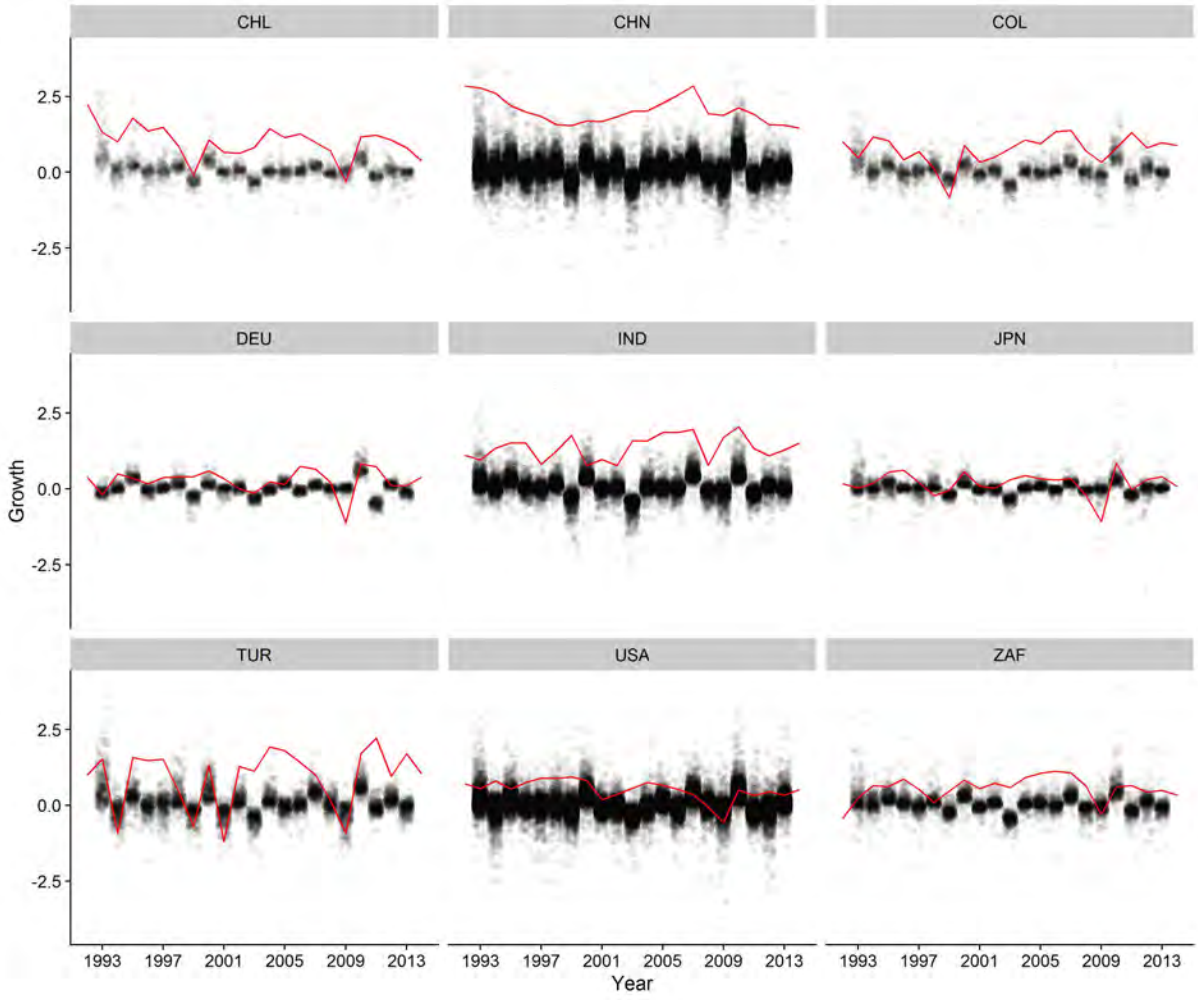

Note: Jitterplots represent annual light growth at the cell level by country. Lineplots represent annual country level GDP growth, scaled by factor 0.2.

activity across the world.

2.2. Natural Disasters

The independent variables of interest measure the physical intensities of geological and meteorological events. Starting from Felbermayr and Gröschl (2014), a new data set of monthly observations is compiled from various sources at 0.5° by 0.5° grid cell resolution for the entire globe, named the Gridded GAME (geological and meteorological events) Database. The database covers the period 1979–2014 and captures earthquakes, storms,

droughts, extreme precipitation and extreme temperature events.[17] While this research will ultimately be at the annual level, it is quintessential to collect primary intensity data at the monthly level for climatic and meteorological events, the lowest common level of disaggregation. This allows accounting for local seasonality in meteorological and climatic patterns. The main objective is to identify extreme events, which by construction implies identifying anomalies from local conditions. The climate science literature is followed in defining anomalies as (extreme) deviations from monthly means for an individual cell (see Kraus, 1977; Nicholson, 1986).

Data from the Incorporated Research Institutions for Seismology (IRIS)[18] is used to measure the locations of epicenters and magnitudes of **earthquakes**.[19] IRIS collects data from a vast number of seismological institutions around the world and provides global coverage. Maximum earthquake magnitudes observed at epicenter locations are mapped to the respective grid cell within a given month. As IRIS provides global coverage, any missing values are set to zero.

Data on **extreme precipitation** events is also collected. These events may cause damage, when precipitation exceeds the local percolation capacities.[20] Monthly precipitation in millimeters stems from the University of East Anglia Climatic Research Unit Timeseries (CRU TS 3.23).[21] The data set is based on gauge data by weather stations. As precipitation can be discontinuous in time and fractal in space, climate scientists apply sophisticated reanalysis methods to produce high-quality estimates for monthly precipitation covering all land areas (excluding Antarctica) at 0.5° resolution (see Harris et al., 2014). CRU compiles and homogenizes station data from numerous sources into a consistent format, assessing global precipitation variability and additional variables that allow the derivation of drought indices, such as the Standardized Precipitation-Evapotranspiration Index (SPEI). To identify extreme precipitation events by cell at the monthly level, location-specific seasonality and systematic spatial differences are taken into account. Following the climatological literature, standardized anomalies are calculated by subtracting the long-run (1979-2014) mean precipitation observed in a cell for

[17]Note that the Gridded GAME data includes records on volcanic eruptions and accompanying Volcanic Explosivity Index (VEI), but since continuous presence of lava at the surface emits light that is captured in the night-light data, no use can be made of this measure in the present study.

[18]http://service.iris.edu/fdsnws/event/docs/1/builder/

[19]Magnitudes provided (e.g., Richter Scale, Moment Magnitude) differ across earthquakes, but all follow a logarithmic scale, are valid in their respective range and can be compared with each other.

[20]Information on flood events (their extent and depth) at the grid cell level, as provided by the Dartmouth Flood Observatory, would be preferred, but no such data is available with global and consistent coverage.

[21]http://browse.ceda.ac.uk/browse/badc/cru/data/cru_ts/cru_ts_3.23/data.

a given month and standardizing it with the corresponding cellular long-run standard deviation for that month:

$$\gamma_{i,m,y}^{prec} = \frac{x_{i,m,y}^{prec} - \bar{x}_{i,m}^{prec}}{\sigma_{i,m}^{prec}}, \text{ where } i = \text{cell}, \; m = \text{month}, \; y = \text{year}.$$

This indicator measures both positive and negative precipitation extremes. As extreme precipitation events which potentially exceed local percolation capacities are of particular interest, the constructed monthly precipitation indicator is censored at zero.[22] The resulting measure records the positive deviation of precipitation from the long-run monthly mean in a cell accounted in units of standard deviation from its mean.

To capture **droughts**, the SPEI is calculated from gridded data on precipitation (PRE) and potential evapotranspiration (PET) contained in the CRU TS 3.23 data set. This takes into account the amount of water coming in (precipitation) and the amount lost (evapotranspiration), resulting in a climatic water balance for each cell in a given month. (Vicente-Serrano et al., 2010) is followed[23] to construct a cell-specific monthly SPEI that has a zero mean, a standard deviation of one and is theoretically unbounded. Negative values indicate drought events, hence, a zero-censored version of the constructed indicator is used.[24] Hot weather conditions enter the SPEI as part of potential evapotranspiration. The drought indicator therefore includes heat waves to the extent that they are accompanied by dry conditions.

Cold waves can cause major disruption to both social and economic activity. To capture these events, gridded 0.5° resolution land surface temperature in degrees Celsius is used[25], compiled by the Climate Prediction Center (CPC) of the National Oceanic and Atmospheric Administration (NOAA). This data set combines two large sources of station observations collected from the Global Historical Climatology Network (GHCN) v2 and the Climate Anomaly Monitoring System (CAMS).[26] To obtain global spatio-temporal coverage and consistency, unique reanalysis methods are applied to the source data (see Fan and Van den Dool, 2008). Again, the grid cell resolution is perfectly

[22]The uncensored precipitation measure is recorded in the Gridded GAME database. While negative index values might hint at droughts, a more sophisticated index proposed in the hydrological literature is used.

[23]The climatic water balance (PRE−PET) is standardized for each cell with a log-logistic distribution function, applying the unbiased probability weighted moments method to data from the current and the respective past $n-1$ months with $n \in [1, 3, 6, 9, 12]$. The reference period to obtain the distribution parameter is 1901–2014.

[24]The converse argument that positive values represent extreme precipitation events is, however, not true.

[25]Mean surface temperatures provided in Kelvin is converted to Celsius: $°\text{C} = °\text{K} - 273.1$

[26]http://www.esrl.noaa.gov/psd/data/gridded/data.ghcncams.html.

consistent with Gridded GAME such that observations are merged by longitude and latitude of cells' geographic centers. Cell-specific low temperature events at the monthly level are identified as standardized anomalies, analogous to extreme precipitation events, by taking location-specific seasonality and systematic spatial differences in the climatology into account. Hence, temperature is normalized by subtracting the long-run (1979-2014) mean temperature observed in a cell for a given month and standardizing this deviation by the cell long-run standard deviation for that month:

$$\gamma_{i,m,y}^{temp} = \frac{x_{i,m,y}^{temp} - \bar{x}_{i,m}^{temp}}{\sigma_{i,m}^{temp}}, \text{ where } i = \text{cell, } m = \text{month, } y = \text{year.}$$

This indicator reflects both positive and negative temperature extremes. To isolate information on cold wave treatment, positive monthly anomalies are censored and negative ones are expressed in absolute terms. The resulting cold wave indicator records negative deviations of surface temperature from the long-run monthly mean at the cell, accounted in units of standard deviation from this mean.

To examine **storms**, a combined measure is created using information on maximum monthly sustained wind speeds from two distinct sources. The International Best Track Archive for Climate Stewardship (IBTrACS) Version v03r09[27] conveys information on moving center-locations with respective wind speeds of tropical cyclones. The Global Summary of the Day (GSOD) statistics[28] contain wind speeds measured at weather stations. The lack of gridded data poses a challenge: The spatial spillover analysis requires a panel which is balanced and provides at least one neighbor per grid cell. Given the impermanence of cyclones and both the uneven spatial distribution and inter-temporal fluctuation of stations, readily available wind speed data is insufficient to provide these ingredients.[29] Moreover, available point-location data does not accommodate the spatial dimension of storms. Consequently, two types of spatial interpolation techniques are applied. A wind field model provided and described in detail by Geiger et al. (2017) is used to generate continuous gridded wind field cells from IBTrACS, which provides distributions of surface wind speeds around hurricane centers. The model uses all available information on wind speed, pressure and direction to compute sustained winds speeds that most likely occurred in cells surrounding available data points. Figure 2 presents hurricane Katrina

[27] http://www.ncdc.noaa.gov/oa/ibtracs/index.php?name=ibtracs-data.

[28] ftp://ftp.ncdc.noaa.gov/pub/data/gsod.

[29] Balancing reduces the sample to cells with at least one station or hurricane center in every period. Simply setting cells with missing wind speed information to zero induces measurement error as a true monthly maximum wind speed of zero is very unlikely. Figure A2 in the Appendix visualizes observational losses resulting from balancing if wind speeds are not interpolated.

as an example of how raw data are transformed to a wind field. To capture summer and

Figure 2: Hurricane Katrina – IBTrACS (l.) vs. Wind Field (r.)

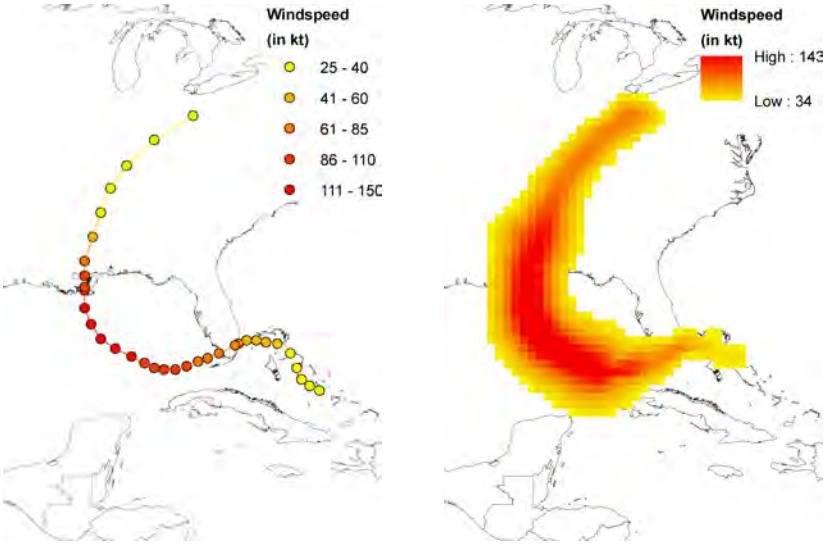

winter storms, cells are filled with gridded non-cyclone wind speeds. GSOD data are combined with a global kriging spatial interpolation algorithm (see Krige, 1951).[30] Finally, a combined wind speed measure is constructed, which prefers wind field information on hurricanes, cyclones or typhoons – if any such event has affected the cell – to the cell's kriged station wind speed. The resulting wind speed indicator is the maximum sustained wind speed for a cell-month combination, measured in knots.

As night-lights are provided annually, the monthly physical intensities are aggregated to an annual intensity indicator for each type. Indicators distributed around zero need to be split, such that extreme events from both tails do not cancel out. Measures of cold waves and droughts need no further adjustment, except censoring positive index values in the monthly data. To aggregate extreme precipitation, negative index values of the monthly precipitation measure are censored.

A straightforward aggregation approach would be to take the simple mean over all monthly observations in a cell for each calendar year. This would, however, introduce measurement error and bias, as all monthly observations within each year would be given

[30]Haslett and Raftery (1989) were the first to adopt kriging to a wind speed context by modeling the spatial distribution of Irish wind power resources using historical wind speed data. Using daily European climate data, Hofstra et al. (2008) show that kriging performs best out of six interpolation methods. Kriged predictions are based on the aerial (semi-)variance in wind speeds across locations in relation to the distance between locations. These predictions convey more information about the spatial persistence of observed values than alternative interpolation methods, e.g., inverse distance weighting, where a linear decay across space is imposed as a structural assumption. The exact procedure is described in detail in Appendix A.2.

the same weight. Consequently, a disaster that occurred earlier in a year may have had a different impact, with respect to the number of months in which luminosity has been captured by the satellites after the event, than one that happened later. To take this dynamic relationship into account, a rolling-window weighted mean for each type is calculated, weighting it by the number of months it affected luminosity. This ensures a uniform take on potential disaster impacts, allowing all realizations to affect light growth for 12 consecutive months.[31] The final indicators capture weighted annual averages of the monthly indicator values from the Gridded GAME database, reflecting disaster intensity by cell and year. Figure 3 describes the distributions of aggregated variables.

Figure 3: Kernel Densities of Annual Aggregate Physical Intensities

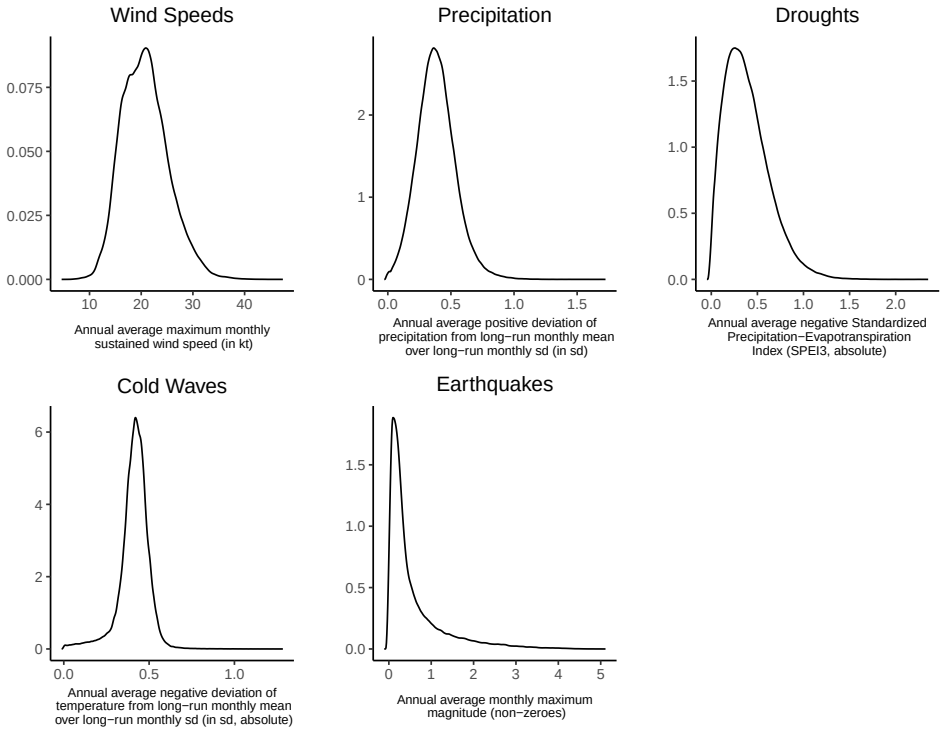

Density distributions of aggregate annual physical intensities. All measures are reported over the full sample, except earthquakes, for which the density over the non-zero magnitudes is reported. Note that 80% of cell-years show zero earthquake magnitude in the full sample.

Note that by construction of the weighted annual average, the range of the distributions is smaller than at the monthly level. Table 1 provides examples of natural events and illustrates how these are reflected in the yearly aggregates in comparison to the monthly

[31] It must be recognized that, in principle, longer lasting disaster impacts are possible. These are taken into account by including a temporal lag of the treatment variable into the regressions. In the robustness section, results are provided which use the simple annual mean as an alternative.

input data. Corresponding cell means and cell standard deviations of the yearly aggregate measure are provided. The examples show that extreme events lie way above the cell means and in the tail of the cell-specific distributions. Full summary statistics on yearly aggregates for the estimation sample are provided in Table A2 in the Appendix.

Table 1: Representation of natural events in the monthly data vs. the yearly aggregates

Event	Date	Place	Lat	Lon	Month	Year	C-Mean	C-SD
Hurricane Katrina	08/2005	New Orleans, USA	28.75	-89.25	138 kt	38.3 kt	28.9 kt	3.4
Odisha Cyclone	10/1999	Odisha, India	19.75	86.25	128 kt	24.8 kt	17.8 kt	3.2
Haiti Earthquake	01/2010	Haiti	18.25	-72.25	7.7	1.3	0.2	0.3
Kobe Earthquake	01/1995	Kobe, Japan	34.75	135.25	7.3	3.8	2.1	0.8
Extreme Rain & Flash-Flood + Heavy Prec. (Ohio Winterstorm)	06/2013 12/2013	Maryville, Missouri, USA	35.75	-83.75	2.66 4.16	1.52	0.43	0.35
Torrential Rains	11/1994	Kairo/Nile Valley, Egypt	30.25	32.25	4.56	0.56	0.23	0.15
UK Record Winter	12/2010	Country-Wide, UK	55.25	-2.25	2.30	0.67	0.43	0.09
Heavy Coldwave	07/2003	Cuzco Region, Peru	-12.75	-71.25	2.04	0.59	0.49	0.11
Drought (prolonged)	01/2012	Country-Wide, Mexico	20.25	-104.25	1.63	0.80	0.52	0.17
Drought (prolonged)	02/1992	Country-Wide, Zimbabwe	-21.25	31.75	2.89	1.38	0.44	0.40

Columns *Lat* and *Lon* represent geographic coordinates of grid cell centroids for reported values. *Month* represents maximum index realizations of respective events in the monthly raw data, observed in the month of occurrence. *Year* represents the corresponding (simple mean) aggregate over 12 months of the year. *C-Mean* and *C-SD* refer to cell-specific distributions of yearly aggregates.

The structure of the disaster intensity variables combined with the fixed effects approach allows letting the data decide which cell-specific events are extreme.[32] It is indeed these (extreme) deviations that form disaster events this research is ultimately interested in.[33]

2.3. Population

A key control variable, population at the pixel level, stem from the Gridded Population of the World (GPW) collection provided by the Center for International Earth Science Information Network (CIESIN). The data contain 5-year target estimates based on census inputs gathered at the lowest administrative units available, which are redistributed from their administrative census boundaries to a uniform pixel grid by using aerial weights.[34] Pixel data are aggregated to grid cell units by summing population numbers within each cell. To interpolate the years between the given 5-year periods, exponential population growth is assumed.

[32]Note that the fixed effects essentially demean the measures, leaving deviations from the cell-mean as the source of disaster identification.

[33]Note that point estimates on the respective disaster variables cannot be directly compared as measures are based on different units of account.

[34]Note that the GPW data applied here is *not* constructed using lights as an input factor; contrary to the widely-used GRUMP population data that make use of night-light emissions to redistribute population counts across pixels.

3. Empirical Strategy

The aim of this research is to identify the local average treatment effect of various types of natural events at the grid level. This requires accounting for the spatial structure of the data both conceptually and econometrically. A grid cell approach is taken with $0.5^\circ \times 0.5^\circ$ resolution. This coincides with primary data records on meteorological and climatological events and provides a natural starting point. Superimposing this arbitrary layout has the advantage that it intersects with actual economic units that may show a high connectivity and clustering. Observational units are therefore entirely exogenous.[35]

A first somewhat naive approach that ignores potential spillovers and the spatial structure of error terms is a simple panel fixed effects growth estimation, in which within-cell variation of year-to-year growth in average night-light emission is related to the intensity of events in that year:[36]

$$\Delta \boldsymbol{\ell_t} = \boldsymbol{\ell_{t-1}} \gamma_{t-1} + \boldsymbol{D_t} \boldsymbol{\beta_t^0} + \boldsymbol{X_t} \boldsymbol{\delta_t^0} + \boldsymbol{\nu} + \boldsymbol{\pi} + \boldsymbol{u_t} \tag{1}$$

where the $K \times 1$ vector $\Delta \boldsymbol{\ell_t}$ captures the growth rate in night-light emissions expressed in yearly changes of the logarithm of mean night-light intensity $\boldsymbol{\ell_t} \equiv \ln\left(\overline{\mathbf{light}_t}\right)$ for each of the K grid cells, $\Delta \boldsymbol{\ell_t} \equiv \boldsymbol{\ell_t} - \boldsymbol{\ell_{t-1}}$. The disaster treatment variable $\boldsymbol{D_t}$ is a $K \times P$ matrix of physical intensities (and temporal lags) and $\boldsymbol{X_t}$ is a $K \times N$ matrix of N control variables (population) at the grid cell level in year t. $\boldsymbol{\pi}$ denotes a full set of year fixed effects to capture global trends, such as technological progress, energy costs, and the global business cycle.[37] Moreover, year fixed effects address systematic time variation in the measurement of light emissions. On-board gain settings of sensors vary across and within satellites over time and with satellite age – yet, these effects are not documented. Accordingly, raw satellite data is not calibrated and direct comparison of light intensities over time would

[35] An alternative would be to conduct estimations at the sub-national level on administrative divisions. Economic data (e.g., income inequality) are available as control variables for some countries. However, these variables are almost always correlated with night-lights, if not (partly) constructed using them. Moreover, administrative units across the globe differ tremendously in size and reflect geographic and demographic conditions as well as political decisions, which are often determinants of night-lights themselves or jointly determined with it.

[36] As more detailed data become available, a higher level of temporal detail may be an alternative. But studying annual averages ensures that not only short-run power outages are captured (a channel through which disaster events might affect night-light emissions) such that the focus is on longer lasting impacts on the emission of night-light throughout the year.

[37] In the sensitivity analysis, it is shown that results remain robust when including country-specific year-effects. While this allows to control for time-varying country characteristics (e.g. institutions, policies or overall infrastructure), it tremendously reduces the degrees of freedom and restricts identification to countries beyond a critical geographic size.

therefore be problematic. This issue is tackled by following Henderson et al. (2012) and Chen and Nordhaus (2011) who propose to include time fixed effects. $\boldsymbol{\nu}$ denote cell fixed effects controlling for time-constant local unobservable variables. Cell fixed effects absorb location-specific baseline risk, which determines to what extent disasters occur unexpectedly and may thus affect economic responses to shocks. Consequently, identification relies on unexpected variation in the physical intensity measure. How night-light growth reflects GDP growth may be structurally related to historical, cultural and political differences in the use of light. In addition, night-light emission patterns may be systematically driven by land use. Areas dominated by agricultural use emit little to no light as they grow (Keola et al., 2015). To the extent that these differences and land use patterns are time-invariant, they are captured by cell fixed effects. Cell fixed effects also control for inherent systematic measurement error in night-lights across latitude (e.g., due to stray light, aurora, and the solar cycle) and for overall topography and other unobserved geographic determinants. This basic model is explored first to take the analysis from national to the grid cell level and to show very basic correlations.

However, the spatial dependence of both night-light growth and disaster intensity requires relaxing the traditional independence assumption, often implicitly applied in most work in this field. As cells intersect true economic units (e.g., cities or metropolitan areas), this makes them spatially dependent by construction. Also, weather shocks typically do not account to only single cells but have a spatial extent of their own. Thus, despite treatment variation across space within this extent, exogenous shocks are correlated with shocks in neighboring cells. In addition, night-light growth in one cell is not orthogonal to disasters occurring in neighboring cells due to potential spillover effects. Hence, treatment of neighbors may have explanatory power and is correlated with own treatment, which leads to omitted variable bias.

To avoid this bias and account for spatial dependence, the idea is to simultaneously model local treatment effects and spillover effects to neighboring cells. Therefore, a spatial Durbin error model (SDEM) (cp. Anselin, 2013; Halleck and Elhorst, 2015) with cell and year fixed effects is chosen.[38] In this model, the dependent variable may not only depend on own covariates but also on the covariates of neighboring units. This implies that natural shock events not only affect light growth in the cells in which they are recorded, but also indirectly affect light growth in neighboring cells. A fully specified spatial panel

[38]As it is reasonable to assume that spatial spillovers from natural events are confined in their geographical extent, local rather than global spillovers are modeled explicitly. This study therefore prefers the SDEM over the more often used spatial Durbin model (SDM) specification. For a discussion, see Halleck and Elhorst (2015). Section 5.5 discusses SDM as an alternative specification.

model is estimated of the form:

$$\begin{aligned} \Delta \boldsymbol{\ell_t} &= \boldsymbol{\ell_{t-1}}\gamma_{t-1} + \boldsymbol{D_t}\boldsymbol{\beta_t^0} + \boldsymbol{X_t}\boldsymbol{\delta_t^0} + \boldsymbol{W^r}\boldsymbol{D_t}\boldsymbol{\beta_t^1} + \boldsymbol{W^r}\boldsymbol{X_t}\boldsymbol{\delta_t^1} + \boldsymbol{\nu} + \boldsymbol{\pi} + \boldsymbol{u_t} \\ \boldsymbol{u_t} &= \rho \boldsymbol{W^r}\boldsymbol{u_t} + \boldsymbol{\varepsilon_t}. \end{aligned} \tag{2}$$

where $\boldsymbol{W^r}$ is a time-invariant $K \times K$ dimensional spatial weights matrix, which allows accounting for spatial spillovers. It is specified as binary and isotropic, meaning that its elements are equal to one for all neighboring cells within the spatial radius r around a given cell's center and discretely drop to zero for all cells beyond that radius, as recommended by Conley (2008).[39] In the baseline specification, a geodesic radius r of 80 km is chosen. This implies that effectively eight adjacent cells are considered neighbors at the equator. Using a constant metric distance ensures that the geographic area of neighbors remains constant over latitude. This leads to the inclusion of a larger number of cells along the longitudinal axis the further one moves away from the equator.[40] Gibbons et al. (2015) discuss requirements of imposing structure on the spatial process to disentangle treatment effects from direct spillovers in the dependent variable. The cutoff choice is to some extent arbitrary and it is not formally testable.[41] By interacting determinants with $\boldsymbol{W^r}$, spatial lags are obtained. The inclusion of spatial lags – similar to the inclusion of temporal lags in time-series – allows local outcomes to depend not only on local treatment but also on the treatment of neighbors. $\boldsymbol{\beta_t^1}$ and $\boldsymbol{\delta_t^1}$ are thus average local spillover effects of a marginal change in the respective explanatory variable in *one* neighboring cell.

Following the econometric literature, spatial clustering and spillovers in unobserved characteristics are accounted for by allowing for spatial auto-correlation in the error term $\boldsymbol{u_t}$. This is crucial due to potentially high connectivity and clustering of observed values in the spatially disaggregated data and to account for the fact that residual spatial auto-correlation (RSA) may reflect unobserved natural or economic processes. Superimposing an arbitrary grid cell layout implies that cells need not be independent from each other, as cell borders may intersect true economic units (i.e., urban settlements) and share national or regional business cycles and institutions. While the imposed spatial structure accounts partially for the true spatial dependence, it must still be corrected for RSA, which otherwise may bias the spatial estimates.

[39] This structure imposes a strict balancing restriction on the panel such that the same set of neighbors is used for a specific cell across all 21 years in the sample.

[40] Due to the curvature of the earth, the metric length of 0.5° longitude decreases with latitudinal distance to the equator, whereas the metric length of 0.5° latitude remains approximately constant.

[41] To test whether results are sensitive to the spatial radius chosen for the weights matrix, the distance cutoff is increased in Section 5.2 to $r = 160$ km.

The Global Moran's I test (Moran, 1950) allows testing for residual auto-regressive processes ($\boldsymbol{u_t} = \rho \boldsymbol{W^r u_t} + \boldsymbol{\varepsilon_t}$).[42] In a spatial lag of X (SLX) regression with two-way cell and time fixed effects, a positive and statistically significant test is observed for all disaster categories, see Table A5. Hence, the Null is rejected in favor of positive RSA (i.e., spatial clustering). Thus, the SDEM is preferred over the more parsimonious SLX specification. To account for RSA, Baltagi et al. (2007) type spatial auto-correlation in the residuals is applied.[43] To model RSA and to address non-linearity in ρ, the Maximum-Likelihood approach for spatial panel models provided by Millo and Piras (2012) and Millo (2014) is used. This allows consistent estimation of the local economic impact of natural disasters together with spillover effects to neighboring locations.

4. Main Results

In this section, a parsimonious panel fixed effects model is taken as a starting point to then show how modeling the spatial dependence of grid cells changes local treatment effects. In later sections, robustness checks are presented and heterogeneity in income groups and across world regions is explored.

4.1. Explorative Results

Following Bertinelli and Strobl (2013) and Elliott et al. (2015), the point of departure is a simple ordinary least squares (OLS) model including cell and year fixed effects, as described in the methodology section. Extreme precipitation is taken as an example, as this shows most explicitly how modeling spatial spillovers affects the results. Results are presented in Table 2, columns (1) to (4). Not accounting for spatial dependence and spatial autocorrelation in the simple panel fixed effects setting suggests a positive and statistically significant effect of precipitation on night-light growth in column (1). This is a counterintuitive finding reminiscent of earlier results in the literature; see Felbermayr

[42] It takes the following form

$$I = \frac{N}{W} \cdot \frac{\sum_c \sum_j w_{cj}(x_c - \bar{x})(x_j - \bar{x})}{\sum_c (x_c - \bar{x})^2}.$$

The Null of no residual spatial auto-correlation equals $E(I) = \frac{-1}{N-1}$.

[43] An SLX model excluding the spatial error component is also estimated. Results are shown in Tables A6 to A8 in the Appendix. Furthermore, an ordinary least squares (OLS) model is estimated with standard errors adjusted for spatial clustering following the procedure implemented by Hsiang (2010), see Table A17.

and Gröschl (2014) for a discussion. Controls, such as initial light levels and population show expected negative and positive results, respectively.

As spatial dependence between grid cells is present, spatial spillovers in production and consumption may affect surrounding locations. Thus, in column (2), Halleck and Elhorst (2015) are followed by estimating an SLX model, which includes the spatial weights matrix but does not account for residual spatial autocorrelation. The local average treatment effect turns substantially negative and highly significant, while simultaneously a positive coefficient estimate for the spatial spillover of extreme precipitation is found. Hence, the local impact of extreme precipitation is negative, but a cell's night-light growth is positively affected by extreme precipitation events in neighboring cells.[44] Point estimates on lagged night-light intensity and population remain stable and highly significant. Next, a temporal lag is added to the SLX model to allow for dynamic effects in column (3). For lagged local treatment and spatial spillovers, highly significant point estimates suggest a reversal of respective effects in the year of occurrence. This indicates that spillovers are, on average, temporary and recovery occurs within two years.

The spatial spillovers modeled capture spatial dependence only partially due to the fact that grid cells may intersect with metropolitan areas along their arbitrary borders. Night-light growth is thus expected to be spatially correlated across contingent cells due to unobserved characteristics which also follow a spatial pattern, so residual spatial autocorrelation remains a concern.[45] Therefore, in column (4), the preferred SDEM model is estimated, which augments the SLX model with Baltagi-type spatial errors. Point estimates on both local and spillover effects are substantially reduced in size but remain qualitatively similar. Note that the lagged spillover effect of extreme precipitation turns insignificant in the SDEM specification. The spatially auto-regressive parameter ρ is positive and highly statistically significant, which is in line with the results of Moran's I test.

To compare obtained estimates with existing grid level studies, the storm indicator is specifically taken under consideration (see Table 2, columns (5) to (8)). In line with Bertinelli and Strobl (2013) and Elliott et al. (2015), local average treatment effects remain consistently negative across all model specifications (also in the lags). Note, however, that

[44] Note that Bertinelli and Strobl (2013) and Elliott et al. (2015) investigate potential spatial spillovers. However, rather than allowing for direct spillovers, they average disaster intensity over the set of a cell and a range of its neighbors. Both studies find little evidence for spatial spillovers, while this study finds strong evidence in favor of their existence. Note that the the size of grid cells (0.5°compared to 1 km^2) is considerably larger. Spatial spillovers in this approach are thus estimated over a much longer distance, while their spillovers would be part of the local treatment effect in this approach.

[45] Absence of RSA is rejected in the SLX model for all disaster types in a Moran's I test, with evidence for positive spatial autocorrelation implying spatial clustering patterns.

Table 2: Model Buildup: Impact of Precipitation and Wind on Light Growth

Dependent Variable: $\Delta \ln(\text{lights}_t)$

	precip.				**wind**			
	(1)	(2)	(3)	(4)	(5)	(6)	(7)	(8)
disaster_t	0.0115***	−0.0613***	−0.0752***	−0.0310***	−0.0051***	−0.0102***	−0.0010	−0.0020**
	(0.0029)	(0.0078)	(0.0081)	(0.0070)	(0.0003)	(0.0009)	(0.0010)	(0.0009)
disaster_{t-1}			0.0481***	0.0219***			−0.0143***	−0.0090***
			(0.0077)	(0.0069)			(0.0010)	(0.0009)
$W \cdot \text{disaster}_t$		0.0114***	0.0138***	0.0049***		0.0008***	−0.0002	0.0000
		(0.0011)	(0.0011)	(0.0013)		(0.0001)	(0.0001)	(0.0002)
$W \cdot \text{disaster}_{t-1}$			−0.0079***	−0.0021			0.0015***	0.0008***
			(0.0011)	(0.0013)			(0.0001)	(0.0002)
$\ln(\text{pop}_t)$	0.0412***	0.0250***	0.0250***	0.0257***	0.0404***	0.0238***	0.0236***	0.0247***
	(0.0028)	(0.0027)	(0.0027)	(0.0013)	(0.0028)	(0.0027)	(0.0027)	(0.0013)
$W \cdot \ln(\text{pop}_t)$		0.0149***	0.0149***	0.0112***		0.0145***	0.0143***	0.0108***
		(0.0009)	(0.0009)	(0.0006)		(0.0008)	(0.0008)	(0.0006)
$\ln(\text{lights}_{t-1})$	−0.4090***	−0.4123***	−0.4122***	−0.4367***	−0.4109***	−0.4146***	−0.4152***	−0.4387***
	(0.0032)	(0.0032)	(0.0032)	(0.0011)	(0.0032)	(0.0032)	(0.0032)	(0.0011)
ρ				0.0672***				0.0672***
				(0.0000)				(0.0000)
Method	OLS	SLX	SLX	SDEM	OLS	SLX	SLX	SDEM
Observations	502,026	502,026	502,026	502,026	507,864	507,864	507,864	507,864

Note: ***, **, * denote significance at the 1%, 5% and 10% level. Specifications (1) to (3) and (5) to (7) are estimated by panel OLS, (4) and (8) is estimated by Maximum Likelihood. Standard errors (in parentheses) allow for heteroskedasticity and clustering at the cell level in specifications (1) to (3) and (5) to (7). Cell and year fixed effects included but not reported. Spatial radius is r=80 km. Yearly disaster intensities reflect time-weighted rolling averages over 12 subsequent monthly observations.

the point estimate for the SDEM specification (column (8)) is more than half the size of that in the OLS specification (column (5)). Contrary to the aforementioned studies, this research finds evidence for positive and statistically significant spatial spillovers. The fact that spillovers show up significantly only in the lagged period may be consistent with results by Bertinelli and Strobl (2013) and Elliott et al. (2015) that suggest absence of spatial spillovers in the contemporaneous year.

Results for all other disaster categories are reported in Tables A6 to A8 in the Appendix. Substantial differences between the estimated local average treatment effect in OLS versus SLX models are found for all disaster categories, and they may vary qualitatively in terms of estimated signs and lagged effects. For all categories but earthquakes, evidence for the presence of spatial spillovers is found. For droughts, the mirror image of precipitation patterns is obtained, with a negative local treatment effect in the OLS, but a sign reversal when allowing for spatial spillovers. Cold waves behave like precipitation, with the sign of the effect reversing when moving from the simple framework to allowing for spatial spillovers. For earthquakes, the size of the positive estimate is reduced together with significance levels when moving from OLS to SLX and subsequently to SDEM, but a positive local treatment effect remains. There is no evidence for consistent spatial spillovers. A reason may be substantial measurement error in the spatial extent of earthquakes and in

their precise location. Reported epicenters often lie at the outer edge of an earthquake's fault rather than at the center of distributed ground movement. Furthermore, capturing negative light growth effects of earthquakes in the yearly response variable might generally be unfeasible: Earthquakes are sudden and short-lived, while temporary relocation of activity into the open, such as evacuation to emergency camps, as well as reconstruction and building sites tend to increase rather than dampen light emissions. Post-impact stimuli to the reconstruction sector are common and are frequently reported (see, e.g., Chang, 2010; Hallegatte and Przyluski, 2010). In addition, duration of the reconstruction phase varies widely, depending on financial and technical constraints (see, e.g., Ghil et al., 2011). For these reasons, further discussion of earthquake results is disregarded in the following. Instead, focus is put on weather shocks, which can be measured with much higher precision in this setup.

4.2. Baseline Results

The previous section clearly established the SDEM model as the preferred specification. Table 3 presents results for each type of weather shock.

Baseline results suggest that storms, extreme precipitation events and cold waves have negative and statistically significant local average treatment effects. Within a geodesic radius of 80 km, significantly positive spatial spillover effects of these event types are observed. This suggests that exogenous shocks lead to a deflection of economic activity towards less affected neighboring regions. Persistence or reversal of treatment effects over time is heterogeneous across disaster types.

Extreme winds that increase the yearly wind speed measure by one knot are associated with a decline in lights growth of 0.2 percentage points on average. Applying the light-to-GDP growth elasticity documented in Section 2.1, a one standard deviation increase in the yearly wind speed measure leads to a reduction of income growth below its local growth path by 0.33 percentage points on average.[46] Interestingly, a large proportion of the growth impact only kicks in with a time-lag. After one period, an increase in the yearly wind speed measure by one knot reduces lights growth by 0.9 percentage points. This implies that a one standard deviation increase in wind speeds reduces economic growth in affected cells by 1.49 percentage points. On average, spatial spillover effects of storms are insignificant in the baseline period. After one period, a positive spillover

[46]The GDP growth effect of a one standard deviation increase in the annual wind measure (4.49) corresponds to a wind speed estimate of -0.0020, multiplied by 100 and translated using the lights-to-gdp growth rate elasticity of 0.37: $[-0.0020 \cdot 100] \cdot 0.37 \cdot 4.49 = -0.33$

Table 3: Baseline Results

Dependent Variable: $\Delta \ln(\text{lights}_t)$

	wind	**precip.**	**drought**	**cold**
disaster_t	−0.0020**	−0.0310***	0.0083*	−0.0762***
	(0.0009)	(0.0070)	(0.0048)	(0.0153)
disaster_{t-1}	−0.0090***	0.0219***	0.0005	−0.0326**
	(0.0009)	(0.0069)	(0.0047)	(0.0149)
$W \cdot \text{disaster}_t$	0.0000	0.0049***	−0.0044***	0.0218***
	(0.0002)	(0.0013)	(0.0009)	(0.0027)
$W \cdot \text{disaster}_{t-1}$	0.0008***	−0.0021	0.0010	−0.0195***
	(0.0002)	(0.0013)	(0.0009)	(0.0026)
$\ln(\text{pop}_t)$	0.0247***	0.0257***	0.0276***	0.0244***
	(0.0013)	(0.0013)	(0.0014)	(0.0013)
$W \cdot \ln(\text{pop}_t)$	0.0108***	0.0112***	0.0115***	0.0106***
	(0.0006)	(0.0006)	(0.0006)	(0.0006)
$\ln(\text{lights}_{t-1})$	−0.4387***	−0.4367***	−0.4329***	−0.4379***
	(0.0011)	(0.0011)	(0.0011)	(0.0011)
ρ	0.0672***	0.0672***	0.0676***	0.0672***
	(0.0000)	(0.0000)	(0.0000)	(0.0000)
Observations	507,864	502,026	468,174	506,037

Note: ***, **, * denote significance at the 1%, 5% and 10% level. All specifications are SDEM and are estimated by Maximum Likelihood. Standard errors in parentheses. Cell and year fixed effects included but not reported. Spatial radius is r=80 km. Yearly disaster intensities reflect time-weighted rolling averages over 12 subsequent monthly observations.

effect is found which suggests an increase in local lights growth by 0.08 percentage points if in *one* of the neighboring cells the yearly mean wind speed is driven up by one knot – implying an increase in income growth by 0.13 percentage points for a one standard deviation increase in wind.[47]

Monthly extreme precipitation may exceed local percolation capacities and potentially cause flooding. A precipitation event that increases the yearly precipitation measure by one standard deviation reduces local income growth by 0.17 percentage points. One period later, recovery leads to a higher growth in local income by 0.12 percentage point increase in local income growth for a one standard deviation increase in the yearly rainfall measure. A one standard deviation increase in extreme precipitation events in one neighboring cell within 80 km leads on average to spillovers increasing local income growth by 0.03 percentage points. Finally, there is no significant evidence that spatial spillovers persist longer than one period after an extreme precipitation event.

Given that droughts primarily affect agricultural outcomes but agricultural production is not associated with light emission in most parts of the world, finding evidence for a

[47]If a storm hits multiple cells simultaneously, aggregate spillovers from the neighborhood accumulate.

negative local impact of droughts on the light-based outcome proxy is not to be expected. In fact, while night-lights typically reflect industrial and services sectors (Doll et al., 2006; Ghosh et al., 2010), as mentioned earlier agriculture (and forestry) emit less or no visible light as they grow (Keola et al., 2015). From a macroeconomic perspective, agricultural production also reflects intermediary inputs to light-emitting industry production and to general consumption.[48] However, while agriculture may be reflected through consumption and intermediary industry output at the country level, the observational units defined for this analysis are less likely to capture such negative secondary effects due to the high geographic resolution. Instead, it is more likely that droughts in rural areas reduce consumption and intermediary industry output in nearby urban areas, located in neighboring cells. Consequently, negative spatial spillovers are expected to be driven by droughts in mostly rural rather than urban cells.

This hypothesis is supported by the data. Estimates suggest that income growth is reduced on average by 0.04 percentage points for each neighboring 0.5° grid cell within a range of 80 km that experiences a one standard deviation increase in drought.To test the hypothesis that this effect is driven by spillovers from rural to urban cells, an unsupervised machine learning algorithm is combined with the pixel-level land use data from the Moderate Resolution Imaging Spectroradiometer (MODIS) 500-m map of global urban extent (Schneider et al., 2009) provided by the Food and Agriculture Organization of the United Nations (FAO), to classify the data into 0.5°×0.5° cells that are predominantly urban (i.e., residential) or non-urban (see Appendix A.4 for more details).[49] Table A1 in the Appendix shows a decomposition of the direct and spillover effects of droughts along this classification. Results suggest that negative spillovers from non-urban to urban cells drive the aggregate spillover, with magnitudes about twice as large as within non-urban neighborhoods. Spillovers within pairs of non-urban cells persist, however, potentially due to residual urban structures in cells classified as non-urban. As expected, no evidence is found for spillovers from urban to non-urban cells and only weak spillovers are found within urban neighborhoods. The positive direct effect is nearly three times as large in urban compared to non-urban cells.

A one standard deviation increase in cold waves reduces income growth by 0.25 per-

[48] Wu et al. (2013) use aggregate night-lights at country level to estimate the extent to which nighttime lights implicitly reflect agricultural production. In a sample of 169 countries observed from 1995 to 2009, their results suggest that the agricultural sector accounts for 25% of total light radiance.

[49] A simple classification approach is also provided, which does not depend on machine learning for classification. This classification gives a 10% share of urban cells, instead of 5% obtained by the clustering approach. It holds similar results. Note that in both cases classification provides an indication of a cell's key type, but does not imply that a cell is *exclusively* urban or non-urban.

centage points in the base period and by 0.10 percentage points after one period. Corresponding spillovers suggest that economic activity is shifted to neighboring locations in the current year, increasing their income growth on average by 0.07 percentage points. The spillover effect of cold waves does not persist over time; instead a sign reversal in a similar order of magnitude is observed.

Control variables consistently show expected signs and significance levels for all weather shocks. A 1% population increase is associated with an increase in lights growth of 2.5 percentage points on average, which implies an increase in GDP growth of 0.9 percentage points. If population in a neighboring cell increases by 1%, local lights grow by 1.1 percentage points, with an average increase in GDP growth of 0.4 percentage points.

Figure 4: Percentile Light Growth Effects of Natural Disasters

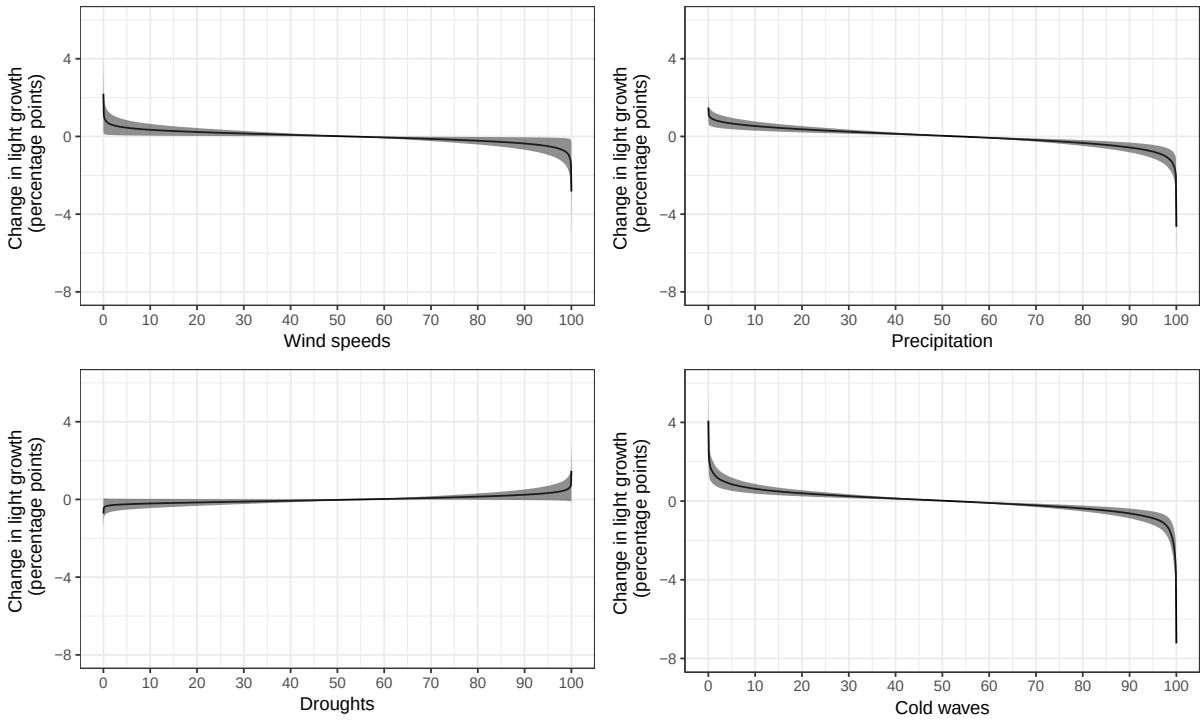

Note: Contemporaneous change in night-light growth as estimated in Table 3, as a function of percentile realizations of the respective demeaned intensity measures (i.e., surprise realizations). 95% confidence interval is plotted in shaded gray.

Next, the distribution of weather shocks is explored to evaluate growth effects at different realizations of respective indicators. Figure 4 shows contemporaneous growth effects along the difference in disaster intensity from its long run cell mean.[50] In line with Fel-

[50]Disaster intensities are demeaned to calculate quantile impacts. The empirical fixed effects strategy

bermayr and Gröschl (2014), a non-linear shape of growth effects is found for all disaster types. This strongly resembles modeling results on the non-linear relation between physical intensity and asset losses or output losses (Hallegatte et al., 2007; Hallegatte, 2008). For all types, the 95% smallest realizations of intensity measures imply a reduction in light growth of less than 1 percentage point.[51] The worst 5% of realizations show substantially larger effects, with extreme shocks being located in the top 1% of realizations. The top 1% of storms decrease light growth by more than 1 percentage point, while the top 1% realizations of extreme precipitation are associated with a reduction in light growth of more than 2 percentage points. The top 1% of cold waves are associated with more than 3 percentage points lower light growth. Drought effects should be treated with caution due to the features discussed above. For completeness, positive drought effects are equally more sizable for the largest 1%, but only weakly significant.

5. Robustness

Next, issues related to measurement and alternative specifications that may affect the baseline results are explored. A summary of robustness results is shown in Table 4.

5.1. Sensitivity to Top- and Bottom-Coding

DMSP satellite sensors are subject to saturation, resulting in top-coding of pixels for which light emission is at or above the sensor's detection saturation level.[52] Pixels are top-coded at DN63 and are mainly found in urban centers. The share of top-coded pixels ranges from zero in some low and middle income economies — but also in sparsely populated high income countries (e.g., Canada) — to around 2.5% for small but densely populated high income areas (e.g., the Netherlands, Belgium). Notable exceptions are Singapore and Hong Kong, both small and densely populated, and two small island states (Malta and Trinidad and Tobago). There, the share of top-coded cells runs close to or within the double digits as a substantial part is urban built-up area.[53]

identifies on surprise realizations of treatment variables. Non-demeaned physical intensities exhibit clustering of non-surprises especially within the lower quantile. Since these do not contribute to identification, demeaning is used to avoid overdrawing growth effects.

[51] Lower percentiles ultimately constitute positive surprise events.

[52] Bluhm and Krause (2017) propose a method to impute "true" light values for top-coded pixels by assuming a Pareto distribution on top lights. Although this approach may be of great value to the general literature, imputed measures cannot be used for studying shocks on its values.

[53] Gas flaring introduces areas with top-coded pixels into the raw data. These are masked by default, as described in the Appendix Section 2.1.

Top-coding may be a concern for identification if the change in night-time lights due to a shock happens beyond the saturation level of the satellite sensor. To account for this, pixels which are top-coded at least once during the observed time period are masked. None of the 0.5° cells are fully top-coded, while 8% of cells in the sample contain some fraction of top-coded pixels. The mean degree of top-coding is 3.7% (sd 8.4%) and for 99% of these cells top-coding is below 50% of land area. As top-coded pixels are unresponsive to shocks as long as light levels remain beyond the satellite sensor saturation threshold, excluding these should – if anything – lead to larger point estimates. Table 4, Panel A shows that results are robust to excluding top-coding from the data, with all disaster models showing point estimates almost identical to the baseline results.[54]

Bluhm and Krause (2017) suggest that satellite sensor saturation starts already at pixel values as low as DN55. While changes in the DN55-DN62 range can still be measured, larger measurement error might be present in this range with a structural downward bias on recorded versus true brightness. If this is the case, growth in night-light intensity is underestimated in the upper range of pixel values, which in practice affects mostly urban centers.[55] Applying the top-coding approach to pixel values above DN55, point estimates are similar to the baseline.[56]

Data quality concerns also exist at the lower end of recorded light intensity. Henderson et al. (2012) discuss the underrepresentation of pixels below DN3. To tackle this, all pixels below DN3 are set to zero. Estimated suggest that the baseline results are robust in Panel B, Table 4 – except the contemporaneous treatment effect of storms turns insignificant.[57] Elvidge et al. (2009) discuss in their methodology on the identification of gas flaring that pixel values below DN8 should potentially be ignored to "eliminate background noise present in the products". While the number of pixels below DN3 affects 0.1% of pixels in the data, the share of pixels between DN1 and DN8 is 7.5%. Masking all pixels in this range affects 23% of grid cells and eliminates all low-lit areas.[58] As this likely introduces sample selection, the following results should be interpreted with caution. For storms, contemporaneous treatment turns insignificant, lagged and spillover effects stay robust. Results on excessive precipitation are similar to the baseline when excluding low lit areas. For droughts, the contemporaneous positive treatment effect turns insignificant, while the lag and spillover structure remain unchanged. As droughts mainly affect rural areas

[54]Table A9 in the Appendix shows full results.

[55]About 20 cells are lost when applying this wider masking range.

[56]Results are shown in Table A10 in the Appendix.

[57]Table A12 in the Appendix presents full results.

[58]See Table A3 in the Appendix for summary statistics on the DN distribution of satellite-years. Full results for setting all pixel values below DN8 to zero are presented in Table A11 in the Appendix.

Table 4: Sensitivity Results

Dependent Variable: $\Delta \ln(\text{lights}_t)$

	wind	**precip.**	**drought**	**cold**
PANEL A: Top-Coding: Excluding Top-Coded Pixels				
disaster_t	−0.0019**	−0.0329***	0.0091*	−0.0752***
	(0.0009)	(0.0070)	(0.0048)	(0.0152)
disaster_{t-1}	−0.0090***	0.0222***	0.0012	−0.0318**
	(0.0009)	(0.0069)	(0.0048)	(0.0149)
$W \cdot \text{disaster}_t$	0.0000	0.0052***	−0.0046***	0.0219***
	(0.0002)	(0.0013)	(0.0009)	(0.0027)
$W \cdot \text{disaster}_{t-1}$	0.0008***	−0.0023*	0.0011	−0.0200***
	(0.0002)	(0.0013)	(0.0009)	(0.0027)
PANEL B: Bottom-coding: Setting Pixels <DN3 to Zero				
disaster_t	−0.0007	−0.0265***	0.0082*	−0.0852***
	(0.0009)	(0.0070)	(0.0048)	(0.0154)
disaster_{t-1}	−0.0106***	0.0290***	0.0015	−0.0291*
	(0.0009)	−0.0069	(0.0048)	(0.0150)
$W \cdot \text{disaster}_t$	−0.0001	0.0042***	−0.0041***	0.0242***
	(0.0002)	(0.0013)	(0.0009)	(0.0027)
$W \cdot \text{disaster}_{t-1}$	0.0010***	−0.0022*	0.0007	−0.0217***
	(0.0002)	(0.0013)	(0.0009)	(0.0027)
PANEL C: Radius r=160km				
disaster_t	−0.0016**	−0.0249***	0.0125***	−0.0849***
	(0.0007)	(0.0057)	(0.0041)	(0.0136)
disaster_{t-1}	−0.0052***	0.0158***	−0.0075*	−0.0129
	(0.0007)	(0.0057)	(0.0040)	(0.0133)
$W \cdot \text{disaster}_t$	0.0000	0.0008**	−0.0015***	0.0061***
	(0.0000)	(0.0004)	(0.0003)	(0.0009)
$W \cdot \text{disaster}_{t-1}$	0.0001*	0.0000	0.0005*	−0.0060***
	(0.0000)	(0.0004)	(0.0003)	(0.0008)
PANEL D: Time Varying Country Characteristics				
disaster_t	0.0004	−0.0312***	0.0062	−0.0360**
	(0.0010)	(0.0070)	(0.0049)	(0.0179)
disaster_{t-1}	−0.0049***	0.0117*	0.0009	−0.0390**
	(0.0010)	(0.0069)	(0.0049)	(0.0175)
$W \cdot \text{disaster}_t$	0.0003**	0.0043***	−0.0041***	0.0165***
	(0.0002)	(0.0013)	(0.0009)	(0.0029)
$W \cdot \text{disaster}_{t-1}$	0.0009***	−0.0022*	0.0017*	−0.0144***
	(0.0002)	(0.0013)	(0.0009)	(0.0028)
PANEL E: Simple Annual Mean of Disasters				
disaster_t	−0.0032***	−0.0289***	0.0243***	−0.0613***
	(0.0007)	(0.0055)	(0.0039)	(0.0137)
disaster_{t-1}	−0.0064***	0.0011	−0.0060	−0.0540***
	(0.007)	(0.0055)	(0.0038)	(0.0133)
$W \cdot \text{disaster}_t$	−0.0002	0.0018*	−0.0037***	0.0337***
	(0.0001)	(0.0010)	(0.0007)	(0.0025)
$W \cdot \text{disaster}_{t-1}$	0.0008***	0.0030***	0.0000	−0.0504***
	(0.0001)	(0.0010)	(0.0007)	(0.0019)
PANEL F: Global Spillovers				
disaster_t	−0.0046***	−0.0279***	−0.0016	−0.0974***
	[−0.0044]	[−0.0259]	[−0.0029]	[−0.0794]
	(0.0007)	(0.0060)	(0.0041)	(0.0122)
disaster_{t-1}	−0.0095***	0.0198***	0.0017	−0.0858***
	[−0.0093]	[0.0189]	[0.0017]	[−0.0908]
	(0.0007)	(0.0059)	(0.0041)	(0.0119)
$W \cdot \text{disaster}_t$	0.0005***	0.0037***	−0.0010*	0.0217***
	[0.0000]	[0.0001]	[−0.0001]	[0.0010]
	(0.0001)	(0.0009)	(0.0006)	(0.0017)
$W \cdot \text{disaster}_{t-1}$	0.0008***	−0.0021**	−0.0001	0.0015
	[0.0000]	[−0.0001]	[0.0000]	[−0.0003]
	(0.0001)	(0.0009)	(0.0006)	(0.0017)

Note: ***, **, * denote significance at the 1%, 5% and 10% level. All specifications are SDEM (except Global Spillovers are SDM) and are estimated by Maximum Likelihood. Standard errors in parentheses. Cell and year fixed effects included but not reported in all specifications. Cell and country-year fixed effects included for the time-varying country characteristics analysis but not reported. Spatial radius is r=80 km. Yearly disaster intensities reflect time-weighted rolling averages over 12 subsequent monthly observations. Simple annual mean uses non-weighted mean over all monthly observations within a year. Global Spillovers show average effects translated with spatial multiplier in square brackets. Full results are shown in Tables A9 to A16 in the Appendix.

– typically low lit – the absence of a local treatment effect indeed suggests that it is not possible to measure these local effects in light growth. For cold waves, contemporaneous treatment turns insignificant, while lagged treatment and spillover effects are robust. Overall, result remain broadly in line when considering top- and bottom-coding of night-time light emission data.

5.2. Sensitivity to Spatial Radius

Next, the choice of the cutoff distance for the weighting matrix is addressed. Thus far, a radial distance cutoff of 80 km has been used to define a cell's local neighborhood. Now the sensitivity of results to a larger search radius of 160 km is checked.

Table 4, Panel C suggest that doubling the neighborhood radius does have little effect on local average treatment effects, while average local spillovers remain qualitatively similar but broadly show a substantial decline in magnitude.[59] Hence, adding cells beyond 80 km to the local neighborhood drives down the average spillover effect per cell observed within this neighborhood. This indicates that spatial spillovers of weather shocks are local phenomena that decline with distance, complying with Tobler's first law of geography (Tobler, 1970).

5.3. Time-Varying Country Characteristics

The baseline specification accounts for all time-constant unobservable cell characteristics and overall global trends (technological change, business cycles). This leaves country-specific fluctuations, such as country-wide policy decisions or institutional change, unaddressed. Thus, country-year fixed effects are applied to absorb unobserved country-time specific variation. Three mechanisms potentially affecting estimates are at play: (1) The smaller the country and hence its number of cells, the larger the share of variation in a cell's growth rate that is absorbed by the country-year fixed effect; (2) within cell variation net of country-specifics only allows for identification of local treatment to the extent that this treatment does not affect a country as a whole (e.g., events which are particularly devastating or geographically dispersed may not be reflected in treatment estimates); and (3) 3,927 degrees of freedom are lost, potentially making identification more difficult. (1) and (2) point to the fact that this strategy favors larger countries over smaller ones and may work better for events that are explicitly local by nature.[60] It is known from the

[59] Table A13 in the Appendix shows full results.

[60] Note that droughts, for example, typically stretch over large areas implying that they may well be ongoing in an entire country, albeit to a varying degree throughout its territory.

empirical literature that the most extreme events can have negative consequences for economic growth at the country level (Cavallo et al., 2013; Felbermayr and Gröschl, 2014). Therefore, point estimates are expected to attenuate.

Table 4, Panel D shows that results are qualitatively robust to the inclusion of country-year fixed effects and show an overall decline in magnitudes.[61] The local effect of storms turns insignificant. Note that hurricanes, typhoons and cyclones form the most extreme events in this category, which often hit small island states for which the cell effect is largely soaked up in the country-year fixed effect. Extreme precipitation results prove robust, with the lagged local treatment effect and current spatial spillovers somewhat reduced in size. The lagged spatial spillover turns weakly significant suggesting a higher precision of estimation. Point estimates on local treatment and spillover effects of droughts and cold waves are smaller – droughts turn insignificant.

5.4. Simple Annual Mean

In this part, the aggregation method is changed by taking the simple annual mean over all months within a year instead of the rolling average. Note that this may introduce systematic measurement error and bias by weighting events which occurred later in the year with the same weight as those that happened earlier. Table 4, Panel E shows very consistent results for all types of weather shocks.[62] While local treatment effects decrease slightly in magnitudes for storms, results are consistent for precipitation and increase by factor 2.9 for droughts and by factor 1.2 for cold waves. Spillover effects are consistent for storms, decrease slightly for precipitation and droughts and increase by one- half for cold waves. Generally, results remain unchanged in sign and significance levels.

5.5. Global Spillover Specification

Thus far, *local* spillover effects have been estimated through SDEM or SLX models. The advantage is that estimated coefficients on spatially lagged explanatory variables can be interpreted directly and in terms of local spillover effects attributed exclusively to exogenous variation within a defined neighborhood. An alternative approach, which has often been used in the applied empirical literature, is the spatial Durbin model (SDM) with a spatially autocorrelated dependent variable rather than a spatial error structure. As discussed by Halleck and Elhorst (2015) and Anselin (2013), this class of model structurally implies a *global* notion of spillover effects. With global spillovers, estimates on

[61] For full results, see Table A14 in the Appendix

[62] Table A15 in the Appendix shows full results.

spatially lagged dependent variables do not reflect only exogenous spillovers from the defined neighborhood, but they structurally represent both, exogenous and endogenous spillovers, with the latter resulting as general equilibrium (GE) effects from the propagation of external effects across all contiguous locations in the universe interconnected by a spatial multiplier.[63]

An advantage of the latter approach is that it explicitly enforces "global" compliance with the stable unit treatment value assumption (SUTVA) by allowing observational units not only to interfere within an exogenously defined neighborhood, but across all contiguous locations. The disadvantage, however, is that exogenous local and endogenous global GE spillover components cannot be disentangled. In this context, allowing for a propagation of exogenous weather shocks across all contiguous cells seems inadequate given the goal of explaining local phenomena at a very disaggregated level. Generally, SDM coefficients on the direct and the spatially lagged explanatory variables cannot be interpreted in a straightforward way.[64] Following this, an assessment is provided of how findings are affected in a global spillover model estimated by maximum likelihood techniques:

$$\Delta \boldsymbol{\ell_t} = \boldsymbol{\ell_{t-1}}\gamma_{t-1} + \lambda \boldsymbol{W^r}\Delta \boldsymbol{\ell_t} + \boldsymbol{D_t}\boldsymbol{\beta_t^0} + \boldsymbol{X_t}\boldsymbol{\delta_t^0} + \boldsymbol{W^r}\boldsymbol{D_t}\boldsymbol{\beta_t^1} + \boldsymbol{W^r}\boldsymbol{X_t}\boldsymbol{\delta_t^1} + \boldsymbol{\nu} + \boldsymbol{\pi} + \boldsymbol{\varepsilon_t}.$$

Table 4, Panel F shows consistent results in sign and overall magnitude but convey a different meaning.[65] To properly disentangle direct and spillover effects, coefficients need to be translated applying the spatial multiplier $(\boldsymbol{I} - \lambda \boldsymbol{W})^{-1} = \boldsymbol{I} + \lambda \boldsymbol{W} + \lambda^2 \boldsymbol{W}^2 + \lambda^3 \boldsymbol{W}^3 + \ldots$, such that the direct effect is reflected in the diagonal and the spillover in the off-diagonal elements of $(\boldsymbol{I} - \lambda \boldsymbol{W})^{-1}[\beta_t^0 + \boldsymbol{W}\beta_t^1]$. Panel F includes the mean of all diagonal elements in square brackets for the direct effects, representing the local average treatment effect comparable to the local spillover specification in the baseline. For direct effects, translated coefficients are similar to point estimates. In contrast, the interpretation of translated spillover coefficients in square brackets is very different from the local spillover baseline. The row-wise mean across all connected (non-sparse) off-diagonal elements captures how a cell is affected on average by treatment of any other cell which is part of its contiguously connected spatial neighborhood, also beyond the imposed radius of 80 km.

In general, the mechanics of the global spillover model allow spillovers to propagate

[63] Contiguity implies that some overlap between the spatial neighborhoods of two given cells in the $\boldsymbol{W^r}$ matrix must exist.

[64] As stated by Halleck and Elhorst (2015), this methodological peculiarity is mostly ignored in applied research.

[65] Table A16 in the Appendix shows full global spillover results.

from one 80 km neighborhood to the next, as long as these neighborhoods are contiguously connected. If neighborhoods are spatially disconnected by gaps larger than 80 km, the desired propagation-effect is interrupted. This is often the case across oceans, seas, large mountain ranges, deserts, and other uninhabited spatial areas. Comparison with Figures A7-A10 shows that, even though the term "global spillovers" might suggest otherwise, the cells in the sample are quite far from being contiguously connected around the world such that the global spillovers reported do not reflect a world-wide propagation but rather a "regional" one. Above all, the extent of such contiguous regions is heterogeneous across space and hardly tractable.

Nevertheless, for some parts of the world, contiguous areas are of considerable size. The small estimate for λ indicates that spillovers phase out quickly across space. As a consequence, the mean magnitude by which a cell is affected by *any* other cell in its contiguous neighboring region is, on average, vanishing compared to the local spillover effects from only the next-door neighbors, estimated in the baseline. These insights essentially support the choice of a local spillover specification to be adequate, both due to the lack of spatial contiguity in the data and given the strong phasing-out of effects across longer distances.

6. Zooming In on Heterogeneity

Up to this point, focus has been on the global average of local weather shock impacts. In a next step, heterogeneity in income groups and across world regions is explored.

6.1. Income Groups

Cells are classified depending on whether they belong to high income or to low (and middle) income countries.[66] Table 5 summarizes the results by showing the combined effects from a set of interaction regressions. Estimates suggest that negative wind effects are driven by low income cells in the year of occurrence and thereafter. The lagged negative effect in low income cells is nearly three times as large as in high income cells. Positive lagged spillover effects occur in both types of cells, but are 1.5 times stronger for those that are poorer. Negative treatment and positive spillover effects for precipitation are entirely driven by low income cells. The positive local treatment effect on droughts

[66]The binary categorization of income groups follows World Bank Lending Groups from year 2000. Cells in high income countries account for 31% of the sample, cells in low and middle income countries account for 69%.

shows only in cells of low income countries, as does the negative spillover effect. In line with the baseline, cold waves show a strong negative effect on light growth in low income cells, associated with a positive spillover effect. In high income cells, cold waves lead to more light growth in the period of occurrence and less thereafter, with negative spillovers in the preceding year. Overall, there is evidence that the baseline local average treatment and spillover effects are generally driven by cells in low and middle income countries. This relates well to findings in the literature that developing and poor countries are particularly vulnerable to the impact of extreme natural events (Raddatz, 2007; Noy and Nualsri, 2011).

Table 5: Income Group Heterogeneity, Combined Effects

Dependent Variable: $\Delta \ln(\text{lights}_t)$

	wind	**precip.**	**drought**	**cold**
high income				
disaster_t	−0.0015	0.0171	−0.0120	0.2442***
	(0.0016)	(0.0118)	(0.0093)	(0.0389)
disaster_{t-1}	−0.0042***	0.0249**	0.0081	−0.0680*
	(0.0015)	(0.0117)	(0.0092)	(0.0384)
$W \cdot \text{disaster}_t$	−0.0001	0.0015	−0.0020	0.0077
	(0.0003)	(0.0021)	(0.0016)	(0.0059)
$W \cdot \text{disaster}_{t-1}$	0.0006**	−0.0040*	0.0029*	−0.0224***
	(0.0003)	(0.0021)	(0.0016)	(0.0059)
low income				
disaster_t	−0.0021*	−0.0534***	0.0147***	−0.1133***
	(0.0011)	(0.0087)	(0.0056)	(0.0169)
disaster_{t-1}	−0.0119***	0.0192**	−0.0010	−0.0193
	(0.0011)	(0.0085)	(0.0055)	(0.0165)
$W \cdot \text{disaster}_t$	0.0001	0.0064***	−0.0052***	0.0191***
	(0.0002)	(0.0016)	(0.0011)	(0.0031)
$W \cdot \text{disaster}_{t-1}$	0.0009***	−0.0007	0.0000	−0.0170***
	(0.0002)	(0.0016)	(0.0010)	(0.0030)
Observations	506,142	500,787	467,691	504,525

Note: ***, **, * denote significance at the 1%, 5% and 10% level. All specifications are SDEM and are estimated by Maximum Likelihood. Cell and year fixed effects and controls as in baseline included but not reported. Spatial radius is r=80 km. Yearly disaster intensities reflect time-weighted rolling averages over 12 subsequent monthly observations. Estimates represent combined effects from adding up coufficients from the interaction terms, significance levels are obtained with a two-sided t-test. Full regressions in Table A18.

6.2. World Regions

Next, cells are categorized into world regions (see Figure A13). Table 6 summarizes results from a set of split-sample regressions. Overall, results show that specific weather shocks are driven by some world regions. In line with the baseline, wind speeds show negative effects on night-light growth in Europe, North America, Latin America and the Caribbean (LATAM), as well as in South-East Asia and the Pacific (SEAP). Except for Europe, the lagged effect of wind persists throughout the following year. Middle Eastern and Northern African (MENA) and Central Asian cells show on average a positive effect in the year of occurrence and a negative effect with a lag. Spillover effects are generally positive in subsequent years (except SEAP) and positive in current years in North America and LATAM. Negative effects from excessive precipitation occur in LATAM, SEAP, MENA and Central Asia. A negative but statistically insignificant local treatment effect is found for Sub-Saharan Africa (SSA). Positive spillover effects stem from MENA, Central Asia and SSA.

Table 6: Heterogeneity Across World Regions

Dependent Variable: $\Delta \ln(\text{lights}_t)$

		Europe	**North America**	**LATAM**	**SEAP**	**Central Asia & MENA**	**SSA**
wind	disaster_t	−0.0034*	−0.0076***	−0.0048**	−0.0032*	0.0061**	0.0011
	disaster_{t-1}	0.0042**	−0.0064***	−0.0064***	−0.0080***	−0.0108***	−0.0011
	$W \cdot \text{disaster}_t$	−0.0002	0.0007*	0.0012**	−0.0001	0.0008	−0.0003
	$W \cdot \text{disaster}_{t-1}$	0.0005*	0.0011***	0.0009*	0.0001	0.0020***	0.0016*
prec.	disaster_t	0.0116	0.0026	−0.0659***	−0.0277*	−0.0348**	−0.0365
	disaster_{t-1}	0.0046	0.0049	0.0483***	0.0021	−0.0305*	0.0200
	$W \cdot \text{disaster}_t$	0.0033	0.0013	−0.0022	0.0014	0.0062**	0.0134*
	$W \cdot \text{disaster}_{t-1}$	0.0016	−0.0037	−0.0034	0.0078*	−0.0042	0.0038
drought	disaster_t	0.0042	−0.0245***	0.0373***	0.0021	−0.0176	0.0102
	disaster_{t-1}	0.0011	0.0049	−0.0493***	0.0349***	0.0221**	0.0454***
	$W \cdot \text{disaster}_t$	−0.0077***	0.0021	−0.0008	−0.0066**	−0.0024	−0.0010
	$W \cdot \text{disaster}_{t-1}$	0.0006	0.0045**	0.0015	−0.0047*	0.0057***	−0.0076
cold	disaster_t	0.0906**	0.0256***	−0.1388***	0.1020***	−0.2588***	0.1513**
	disaster_{t-1}	−0.0858*	−0.1636***	−0.0140	0.1289***	−0.4732***	−0.0437
	$W \cdot \text{disaster}_t$	0.0295***	0.0111	0.0117**	−0.0104	0.0455***	−0.0080
	$W \cdot \text{disaster}_{t-1}$	−0.0283***	0.0022	0.0086*	−0.0021	−0.0196**	−0.0152

Note: ***, **, * denote significance at the 1%, 5% and 10% level. All specifications are SDEM and are estimated by Maximum Likelihood. Cell and year fixed effects and controls as in baseline included but not reported. Spatial radius is r=80 km. Yearly disaster intensities reflect time-weighted rolling averages over 12 subsequent monthly observations. Separate regressions for each disaster type and region. Full regressions in Tables A19 – A24.

Droughts reduce night-light growth in North America, while the positive baseline effect is driven by Latin American and Caribbean cells. Negative spillovers of droughts show up in Europe and SEAP. Already very dry regions, such as SSA or MENA show very little

average effects on droughts.

In Europe, North America, SEAP and SSA, cold waves show positive local effects on night-light growth. While Europe and North America can generally afford the technology for coping with the cold, SEAP, as well as SSA benefit from cooler weather as overall warmer regions. Negative local effects from cold waves stem solely from LATAM, MENA and Central Asia. Positive spillover effects from cold waves are driven by Europe, LATAM, MENA and Central Asia.

7. Conclusion

This paper contributes to the emerging literature on the economic consequences of exogenous extreme natural events by taking the debate to the local level, asking how their economic effects propagate across space and time. Satellite night-time light data from 1992 to 2013 are deployed to proxy for local economic activity, which are proven to be highly correlated with GDP growth, and disaggregated seismologic, climatic and meteorologic data on natural disaster events are compiled. Available economic variables, such as light emission and population, are mapped together with the various disaster types on a balanced $0.5^\circ \times 0.5^\circ$ grid. Utilizing maximum likelihood techniques, the impact of various types of exogenous shocks on the growth of night-time light emissions is estimated in a fixed effects setup, controlling for cell population and spatial autocorrelation in the error term. This setup allows explicit modeling and investigation of local average treatment effects but also of spatial spillover effects in nearby locations. With this setup, the problem of varying country sizes or subnational entities as the unit of observation is eliminated.

Results are heterogeneous across the various disaster types. Baseline results show that storms, cold waves and extreme precipitation events reduce local light growth and have positive contemporaneous or lagged spatial spillover effects within a geodesic radius of 80 km. Evaluated along the lights-to-GDP growth elasticity, a one standard deviation increase in wind speeds reduces contemporaneous income growth by 0.33 percentage points. In the next period, the effect quadruples and local spillovers from treatment of *one* neighboring cell increase lights growth by 1.48 percentage points. Likewise, a one standard deviation increase in excessive precipitation or cold waves decreases current income growth by 0.17 or 0.25 percentage points, respectively. In the next period, GDP growth increases on average by 0.12 percentage points due to high precipitation, but persistently decreases by 0.11 percentage points after a cold spell. Associated contemporaneous spillovers total 0.03 and 0.07 percentage points per neighbor treated, respectively. The link between

light emission and droughts is rather weak as they mostly affect agricultural outcomes. Hence, negative spatial spillover effects of droughts are largely driven by rural rather than urban cells. Due to measurement error in the data or temporary relocation of activity into the open combined with reconstruction after an earthquake, a consistent pattern for earthquake events cannot be identified. Overall, results are largely robust to top- and bottom-coding, the spatial radius, the temporal aggregation method, the inclusion of time-varying country fixed effects or the use of a global spillover model.

Finally, some heterogeneity of disaster impacts across world regions and across income groups is shown. In particular, estimates suggest that cells in low and middle income countries drive the baseline results.

References

Anbarci, N., Escaleras, M., Register, C. A., 2005. Earthquake fatalities: the interaction of nature and political economy. Journal of Public Economics 89 (9-10), 1907–1933.

Anselin, L., 2013. Spatial Econometrics: Methods and Models. Vol. 4. Springer Science & Business Media.

Baltagi, B. H., Song, S. H., Jung, B. C., Koh, W., 2007. Testing for Serial Correlation, Spatial Autocorrelation and Random Effects Using Panel Data. Journal of Econometrics 140 (1), 5–51.

Bertinelli, L., Strobl, E., 2013. Quantifying the Local Economic Growth Impact of Hurricane Strikes: An Analysis from Outer Space for the Caribbean. Journal of Applied Meteorology and Climatology 52 (8), 1688–1697.

Bleakley, H., Lin, J., 2012. Portage and Path Dependence. Quarterly Journal of Economics 127 (2), 587–644.

Bluhm, R., Krause, M., 2017. Top Lights Bright Spots and Their Contribution to Economic Development. Mimeo University of Hamburg.

Cavallo, E., Galiani, S., Noy, I., Pantano, J., 2013. Catastrophic Natural Disasters and Economic Growth. Review of Economics and Statistics 95 (5), 1549–1561.

Cavallo, E., Noy, I., et al., 2011. Natural Disasters and the Economy — A Survey. International Review of Environmental and Resource Economics 5 (1), 63–102.

Chang, S. E., 2010. Urban disaster recovery: a measurement framework and its application to the 1995 kobe earthquake. Disasters 34 (2), 303–327.

Chen, X., Nordhaus, W. D., 2011. Using Luminosity Data as a Proxy for Economic Statistics. Proceedings of the National Academy of Sciences 108 (21), 8589–8594.

Conley, T. G., 1999. GMM Estimation with Cross Sectional Dependence. Journal of Econometrics 92 (1), 1–45.

Conley, T. G., 2008. Spatial econometrics. In: Durlauf, S. N., Blume, L. E. (Eds.), The New Palgrave Dictionary of Economics. Palgrave Macmillan, Basingstoke.

Costinot, A., Donaldson, D., Smith, C., 2016. Evolving Comparative Advantage and the Impact of Climate Change in Agricultural Markets: Evidence from 1.7 Million Fields Around the World. Journal of Political Economy 124 (1), 205–248.

Desmet, K., Nagy, D. K., Rossi-Hansberg, E., 2018. The geography of development. Journal of Political Economy 126 (3), 903–983.

Doll, C. N., Muller, J.-P., Morley, J. G., 2006. Mapping Regional Economic Activity from Night-Time Light Satellite Imagery. Ecological Economics 57 (1), 75–92.

Donaldson, D., Storeygard, A., 2016. The View from Above: Applications of Satellite Data in Economics. Journal of Economic Perspectives 30 (4), 171–98.

Elliott, R., Strobl, E., Sun, P., 2015. The Local Impact of Typhoons on Economic Activity in China: A View from Outer Space. Journal of Urban Economics 88, 50–66.

Elvidge, C. D., Ziskin, D., Baugh, K. E., Tuttle, B. T., Ghosh, T., Pack, D. W., Erwin, E. H., Zhizhin, M., 2009. A Fifteen Year Record of Global Natural Gas Flaring Derived from Satellite Data. Energies 2 (3), 595–622.

Fan, Y., Van den Dool, H., 2008. A Global Monthly Land Surface Air Temperature Analysis for 1948–Present. Journal of Geophysical Research: Atmospheres 113 (D1).

Felbermayr, G., Gröschl, J., 2014. Naturally Negative: The Growth Effects of Natural Disasters. Journal of Development Economics 111, 92–106.

Geiger, T., Frieler, K., Bresch, D. N., 2017. A Global Historical Data Set of Tropical Cyclone Exposure (TCE-DAT). Earth System Science Data 10.

Ghil, M., Yiou, P., Hallegatte, S., Malamud, B., Naveau, P., Soloviev, A., Friederichs, P., Keilis-Borok, V., Kondrashov, D., Kossobokov, V., et al., 2011. Extreme events: dynamics, statistics and prediction. Nonlinear Processes in Geophysics 18 (3), 295–350.

Ghosh, T., Elvidge, C., Sutton, P. C., Baugh, K. E., Powell, R., Anderson, S., others, 2010. Shedding Light on the Global Distribution of Economic Activity. Open Geography Journal.

Gibbons, S., Overman, H. G., Patacchini, E., 2015. Spatial Methods. Handbook of Regional and Urban Economics 5, 115–168.

Halleck, V. S., Elhorst, J. P., 2015. The SLX Model. Journal of Regional Science 55 (3), 339–363.

Hallegatte, S., 2008. An adaptive regional input-output model and its application to the assessment of the economic cost of katrina. Risk analysis 28 (3), 779–799.

Hallegatte, S., Hourcade, J.-C., Dumas, P., 2007. Why economic dynamics matter in assessing climate change damages: illustration on extreme events. Ecological economics 62 (2), 330–340.

Hallegatte, S., Przyluski, V., 2010. The economics of natural disasters: concepts and methods. World Bank Policy Research Working Paper No. 5507.
URL https://ssrn.com/abstract=1732386

Harris, I., Jones, P., Osborn, T., Lister, D., 2014. Updated High-Resolution Grids of Monthly Climatic Observations – The CRU TS3. 10 Dataset. International Journal of Climatology 34 (3), 623–642.

Haslett, J., Raftery, A. E., 1989. Space-Time Modeling with Long-Memory Dependence: Assessing Ireland's Wind Power Resource. Applied Statistics, 1–50.

Henderson, J. V., Squires, T., Storeygard, A., Weil, D., 2017. The Global Distribution of Economic Activity: Nature, History, and the Role of Trade. Quarterly Journal of Economics 133 (1), 357–406.

Henderson, J. V., Storeygard, A., Weil, D. N., 2012. Measuring Economic Growth from Outer Space. American Economic Review 102 (2), 994–1028.

Hiemstra, P., Pebesma, E., Twenh"ofel, C., Heuvelink, G., 2008. Real-Time Automatic Interpolation of Ambient Gamma Dose Rates From the Dutch Radioactivity Monitoring Network. Computers & Geosciences.

Hodler, R., Raschky, P. A., 2014. Regional Favoritism. Quarterly Journal of Economics 129 (2), 995–1033.

Hofstra, N., Haylock, M., New, M., Jones, P., Frei, C., 2008. Comparison of Six Methods for the Interpolation of Daily European Climate Data. Journal of Geophysical Research: Atmospheres 113 (D21).

Hsiang, S. M., 2010. Temperatures and Cyclones Strongly Associated with Economic Production in the Caribbean and Central America. Proceedings of the National Academy of Sciences 107 (35), 15367–15372.

Hsieh, C.-T., Ossa, R., 2016. A Global View of Productivity Growth in China. Journal of International Economics 102, 209–224.

IPCC, 2014. Climate Change 2014: Synthesis Report. Contribution of Working Groups I, II and III to the Fifth Assessment Report of the Intergovernmental Panel on Climate Change. [Core Writing Team, Pachauri, R.K., Meyer, L.A. (Eds.)]. IPCC, Geneva, Switzerland, 151.

Kahn, M. E., 2005. The Death Toll from Natural Disasters: The Role of Income, Geography, and Institutions. Review of Economics and Statistics 87 (2), 271–284.

Keola, S., Andersson, M., Hall, O., 2015. Monitoring Economic Development from Space: Using Night-Time Light and Land Cover Data to Measure Economic Growth. World Development 66, 322–334.

Klomp, J., Valckx, K., 2014. Natural disasters and economic growth: A meta-analysis. Global Environmental Change 26, 183–195.

Kraus, E., 1977. Subtropical Droughts and Cross-Equatorial Energy Transports. Monthly Weather Review 105 (8), 1009–1018.

Krige, D. G., 1951. A Statistical Approach to Some Basic Mine Valuation Problems on the Witwatersrand. Journal of the Southern African Institute of Mining and Metallurgy 52 (6), 119–139.

Michalopoulos, S., Papaioannou, E., 2013. Pre-Colonial Ethnic Institutions and Contemporary African Development. Econometrica 81 (1), 113–152.

Michalopoulos, S., Papaioannou, E., 2014. National Institutions and Subnational Development in Africa. Quarterly Journal of Economics 129 (1), 151–213.

Millo, G., 2014. Maximum Likelihood Estimation of Spatially and Serially Correlated Panels with Random Effects. Computational Statistics & Data Analysis 71, 914–933.

Millo, G., Piras, G., 2012. SPLM: Spatial Panel Data Models in R. Journal of Statistical Software 47 (1), 1–38.

Moran, P. A., 1950. Notes on Continuous Stochastic Phenomena. Biometrika 37 (1/2), 17–23.

Nicholson, S. E., 1986. The Spatial Coherence of African Rainfall Anomalies: Interhemispheric Teleconnections. Journal of Climate and Applied Meteorology 25 (10), 1365–1381.

Nordhaus, W., Chen, X., 2015. A Sharper Image? Estimates of the Precision of Night-Time Lights as a Proxy for Economic Statistics. Journal of Economic Geography 15 (1), 217–246.

Noy, I., 2009. The Macroeconomic Consequences of Disasters. Journal of Development Economics 88 (2), 221–231.

Noy, I., Nualsri, A., 2011. Fiscal Storms: Public Spending and Revenues in the Aftermath of Natural Disasters. Environment and Development Economics 16 (1), 113–128.

Pinkovskiy, M., Sala-i Martin, X., 2016. Lights, Camera ... Income! Illuminating the National Accounts-Household Surveys Debate. Quarterly Journal of Economics 131 (2), 579–631.

Raddatz, C., 2007. Are External Shocks Responsible for the Instability of Output in Low-Income Countries? Journal of Development Economics 84 (1), 155–187.

Schneider, A., Friedl, M. A., Potere, D., 2009. A new map of global urban extent from modis satellite data. Environmental Research Letters 4 (4), 044003.

Schneider, F., 2005. Shadow Economies Around the World: What Do We Really Know? European Journal of Political Economy 21 (3), 598–642.

Schneider, F., Enste, D. H., 2000. Shadow Economies: Size, Causes, and Consequences. Journal of Economic Literature 38 (1), 77–114.

Scrucca, L., Fop, M., Murphy, T. B., Raftery, A. E., 2016. mclust 5: clustering, classification and density estimation using Gaussian finite mixture models. The R Journal 8 (1), 205–233.

Storeygard, A., 2016. Farther on Down the Road: Transport Costs, Trade and Urban Growth in Sub-Saharan Africa. Review of Economic Studies 83 (3), 1263–1295.

Strobl, E., 2011. The Economic Growth Impact of Hurricanes: Evidence from US Coastal Counties. Review of Economics and Statistics 93 (2), 575–589.

Strömberg, D., 2007. Natural Disasters, Economic Development, and Humanitarian Aid. Journal of Economic Perspectives 21 (3), 199–222.

Tanaka, K., Keola, S., 2017. Shedding Light on the Shadow Economy: A Night-Time Light Approach. Journal of Development Studies 53 (1), 32–48.

Tobler, W. R., 1970. A Computer Movie Simulating Urban Growth in the Detroit Region. Economic Geography 46 (sup1), 234–240.

Vicente-Serrano, S. M., Beguería, S., López-Moreno, J. I., 2010. A Multiscalar Drought Index Sensitive to Global Warming: The Standardized Precipitation Evapotranspiration Index. Journal of Climate 23 (7), 1696–1718.

World Bank, United Nations, 2010. Natural Hazards, UnNatural Disasters: The Economics of Effective Prevention. The World Bank.

Wu, J., Wang, Z., Li, W., Peng, J., 2013. Exploring Factors Affecting the Relationship Between Light Consumption and GDP Based on DMSP/OLS Night-Time Satellite Imagery. Remote Sensing of Environment 134, 111–119.

A. Technical Appendix

A.1. Supplementary Information: DMSP Night-Lights Data

The United States Air Force DMSP satellites were originally used to detect moonlit clouds, with lights from human settlements being a byproduct that is recorded by the DMSP Operational Linescan System sensor on-board. The sensor records light intensity with a DN between 0 and 63.

Satellites have been observing every location of the planet daily between 8.30 pm and 10 pm local time between 1992 and 2013. Each satellite orbits the earth 14 times a day and thus ensures global coverage every 24 hours (Doll, 2008).

The satellites have a 3000 km swath, from which data of the center half is used to produce images at a nominal resolution of 0.56 km. The data is smoothed on-board to produce an average of 5×5 pixel blocks resulting in a data resolution of approximately 2.7 kilometers at the equator. After smoothing, the data is delivered at a resolution of 30 arc seconds, representing half a minute, or 1/120th of a degree. This gives data for approximately 0.86 square kilometers at the equator, with surface area decreasing in absolute terms when moving away from the equator.

The Earth Observation Group of NOAA then processes the raw data using an advanced algorithm, which cleans the raw data as follows: lights from the center half of the 3000 km swath are selected since these have better geolocation, are smaller and have more consistent radiometry (Earth Observation Group, 2016).

Sunlit data and glare are then excluded based on the solar elevation angle and similarly moonlit data is excluded on basis of the moonlit half of the lunar cycle. Subsequently only cloud-free observations are included and lighting features from the aurora are excluded from the data (Baugh et al., 2010). The exclusion of lighting from auroral features, which concerns high-latitude zones, affects approximately 10,000 people or 0.0002% of the world population (Henderson et al., 2012b, p. 998).

Finally, ephemeral events such as forest fires and other background noise are removed to produce stable average visible light products that reflect annual average human produced light emission into space at a 30 arc second resolution between 65°South and 75°North (Earth Observation Group, 2016). The average number of valid nights for a given pixel in the satellite-years is 39.2 (Keola et al., 2015) and typically ranges between 20 to 100 (Elvidge et al., 2009b).

The share of unlit pixels ranges from only 1% in the Netherlands to 99.47% and 99.89% for the sparsely populated countries Mozambique and Canada (Henderson et al., 2012b, p.

1000). A contrasting example to Mozambique and Canada can be found when comparing Bangladesh and the Netherlands. Both have high population density, Bangladesh having twice the density of the Netherlands with an average of 1,080 people per square km between 1992-2008. Yet, average light intensity – the average digital number per country – is only 2 for Bangladesh, whereas it is 23.5 in the Netherlands (Henderson et al., 2012, p. 1000). With GDP per capita (purchasing power parity, constant 2005 dollars) being 35 times higher in the Netherlands, this indicates that light intensity informs not only about whether there is human life present in a certain area, but also about these areas' relative income per capita (see e.g., Elvidge et al, 2009; Gosh et al. 2010).

Figure A1: Night light emission of Europe and 0.5° grid cells

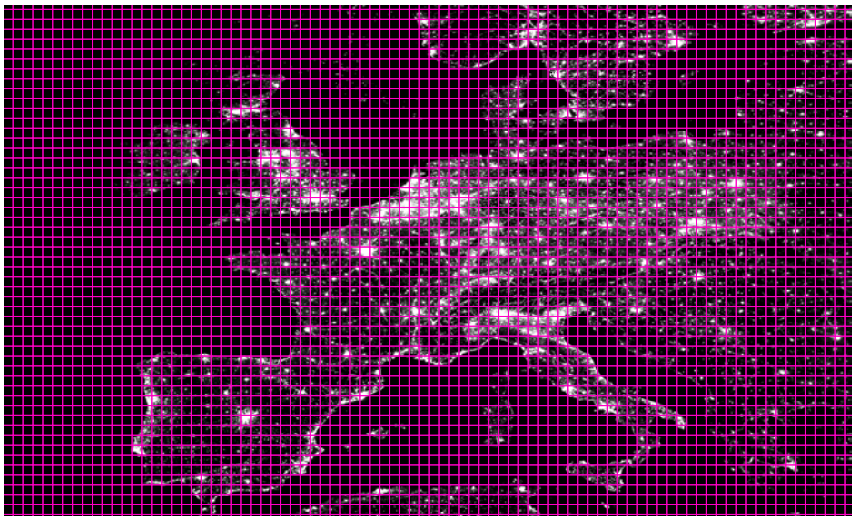

Night light data cleaned and prepared as described. Raw data comes from satellite F182010.

Notwithstanding, a direct comparison of average light intensity can be misleading when not taking into account population size in a given area: The average light intensity of Canada is lower than that of Bangladesh while income per capita is much higher in Canada. Moreover, light usage per person may vary across countries due to cultural differences in night light use and customs of timing of economic activity across day and night. This is why (Henderson et al., 2012) stress that night light intensity is better used as a proxy for income growth rather than income levels. Hence, this approach is followed.

A.2. Interpolation of Wind Speeds

Using the algorithm by Hiemstra et al. (2008), the data are first classified into bins by breaking up distances $\boldsymbol{d}$ between all point locations of weather stations. For each distance bin $\bar{\boldsymbol{d}}$, the cross-sectional empirical (or experimental) semi-variance of observed maximum wind speeds across its n observations at any given point in time is defined by equation (3). $z(x_i)$ is a random function defining a set of random variables, representing the respective wind speeds in any given location x_i. By assumption, the correlation between two random variables $z(x_i)$, $z(x_j)$ depends only on their bilateral spatial distance, irrespective of their location (i.e., stationarity of the second moment of $z(x_i)$). Thus, $z(x_i + \bar{\boldsymbol{d}})$ captures the wind speed realizations observed $\bar{\boldsymbol{d}}$ distance units away from location x_i.

$$\hat{\gamma}(\bar{\boldsymbol{d}}) = \frac{1}{2} \cdot \frac{1}{n(\bar{\boldsymbol{d}})} \sum_{i=1}^{n(\bar{\boldsymbol{d}})} (z(x_i + \bar{\boldsymbol{d}}) - z(x_i))^2 \tag{3}$$

Since the empirical semi-variogram cannot be computed at all possible distances $\boldsymbol{d}$, a model function is fit for each period, for which parameters are fully determined by the data. The best fit in line with the experimental semi-variogram is achieved by the Stein (1999) parametrization of the Matérn model[67] (4) with gamma function Γ and a modified Bessel function K_ν. The nugget (the intercept of the fit) is fixed at zero.[68] σ^2 is the so-called *sill* of the model, which under stationarity of the second moment is simply an estimate of the variance $Var\left[z(x_i)\right]$. ν and κ are non-negative smothing and range parameters, respectively. All parameters are determined by available global wind speed data for any given month.

$$\gamma(\boldsymbol{d}) = \begin{cases} 0 & \text{if } |\boldsymbol{d}| = 0 \\ \sigma^2 \left[1 - \frac{1}{2^{\nu-1}\Gamma(\nu)} \left(2\frac{|\boldsymbol{d}|\sqrt{\nu}}{\kappa} \right)^{\nu} K_\nu \left(2\frac{|\boldsymbol{d}|\sqrt{\nu}}{\kappa} \right) \right] & \text{if } 0 < |\boldsymbol{d}|,\ \nu > 0 \end{cases} \tag{4}$$

The resulting functional fit increases monotonically as a function of distance and is deployed to spatially interpolate the maximum wind speed for any location on the global grid. Note that this interpolation technique allows mapping recorded wind speeds to surrounding locations. For areas that are very sparsely covered with weather stations, this inevitably results in a smoothing effect over larger distances. Note that this introduces

[67] Five different variogram models (spherical, exponential, Gaussian, Matérn, and M. Stein's parametrization of the Matérn model) are tested. Note that the Matérn model includes the exponential model as a special case and the Gaussian model as a limit case ($\nu \lim\inf$).

[68] A zero nugget constrains deviation of predicted from preserved values at very short distances.

a downward bias in the recorded wind speeds, such that obtained estimates may be considered a lower bound. Full global coverage is achieved by using all stations within a geodesic search radius of 2,000 km as predictors. Figure A3 shows the semi-variogram obtained for June 2012. Figure A4 visualizes the corresponding spatially interpolated maximum wind speeds and Figure A5 assesses the fit of these predicted values, using a leave-one-out technique.

Figure A2: Balancing Windspeeds – Cells lost when balancing on non-interpolated wind speed data are shown in red.

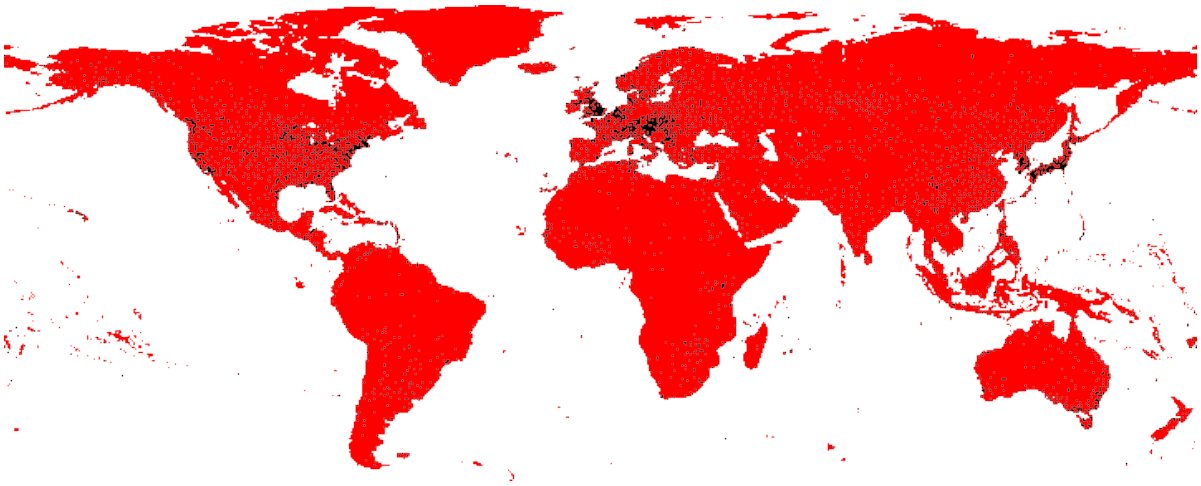

Figure A3: Semi-Variogram for June 2012. Distance is in meters, value labels report the number of bilateral station-distance-pairs per bin.

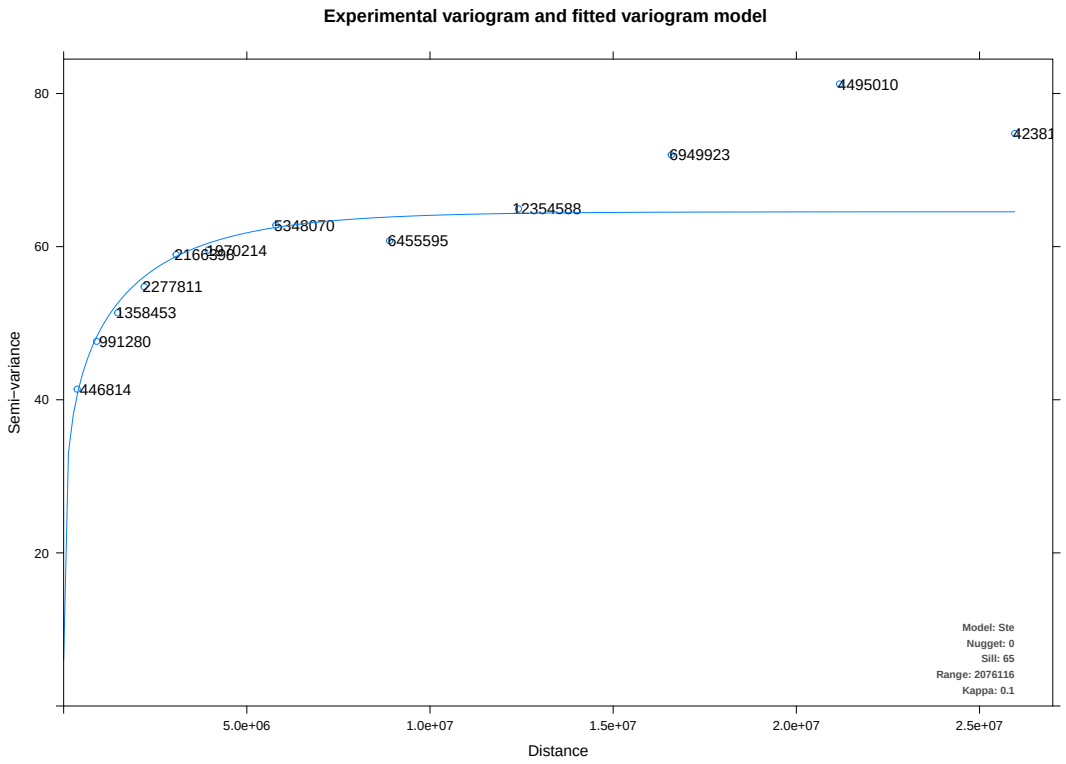

Figure A4: Kriged maximum wind speed in June 2012

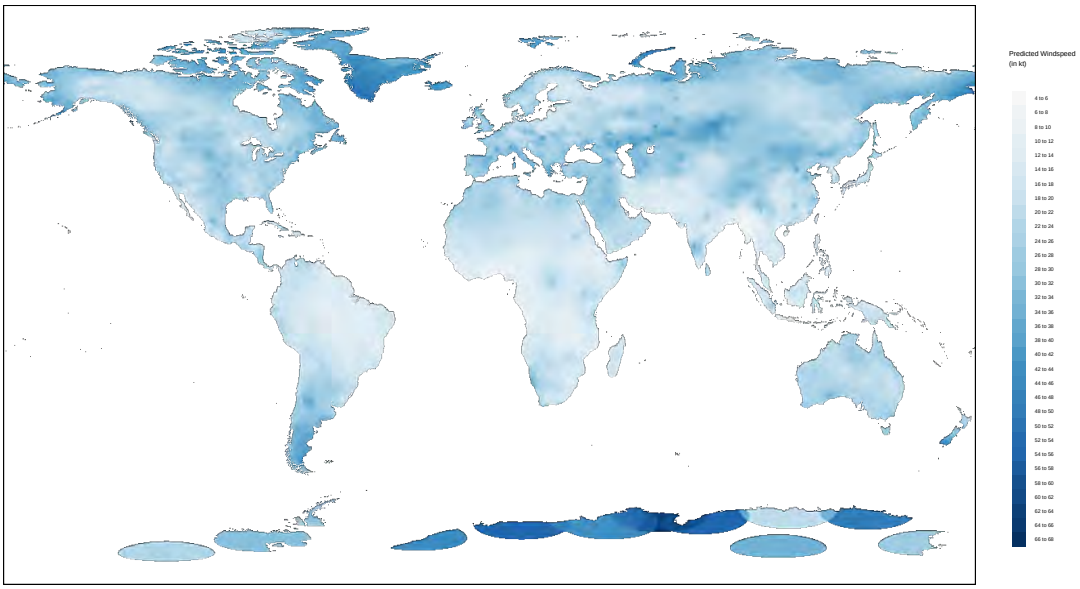

Figure A5: Goodness of fit – Standard deviation of Kriged maximum wind speed (in kt) in June 2012, obtained using the 'leave one out' technique.

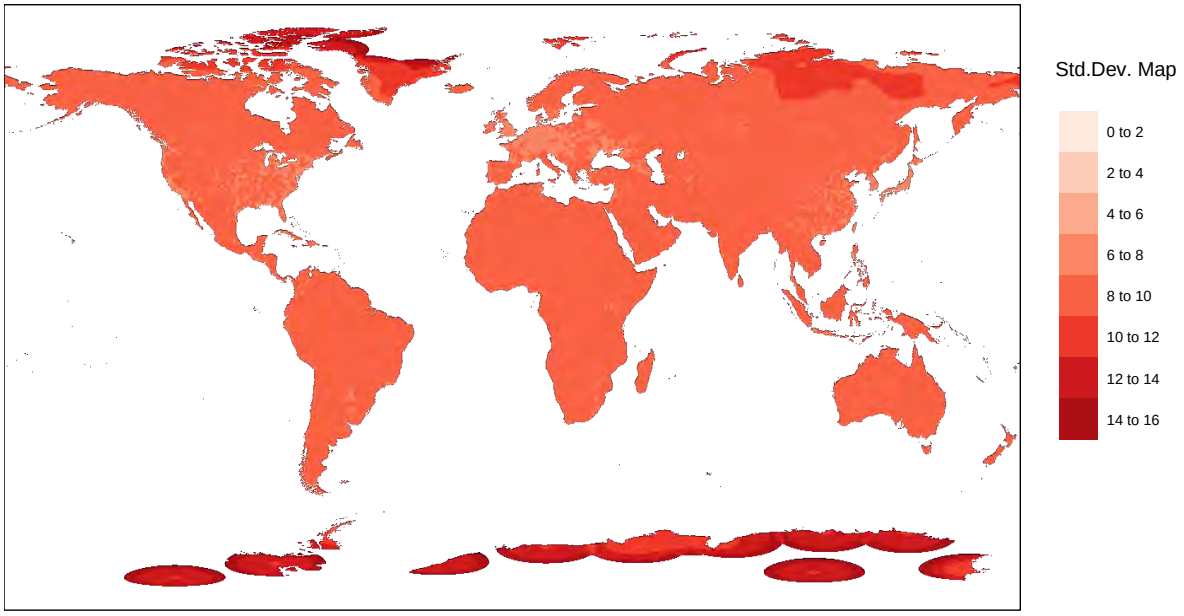

Figure A6: Spiked pattern obtained with inverse distance weighting as alternative choice of wind speed interpolation.

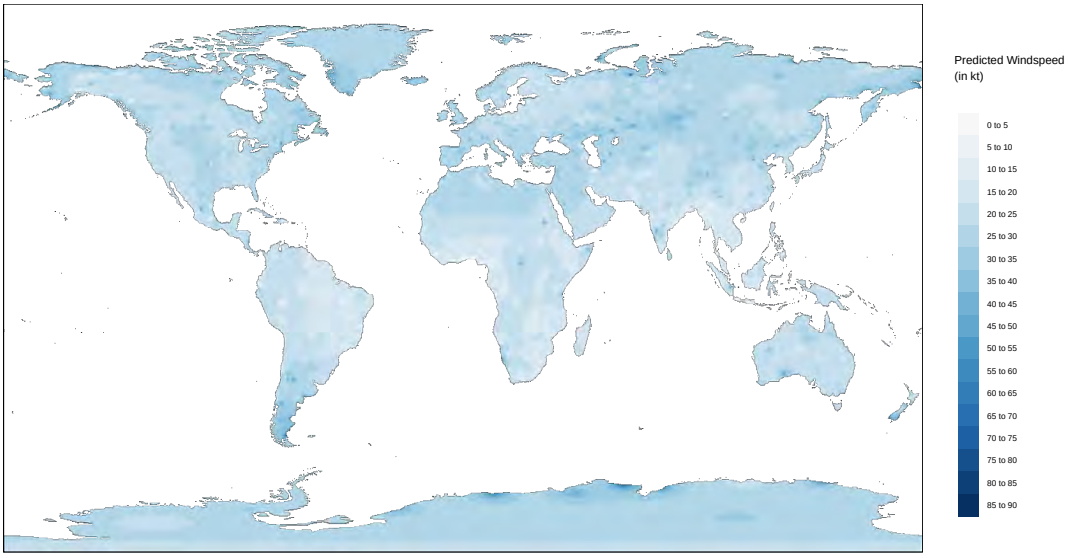

A.3. Balancing

Figure A7: Global distribution of grid cells preserved in balanced panel. Physical indicators used for balancing: Winds. Red: Dropped because of zero absolute light emission in at least one period. Yellow: Dropped because of zero population in at least one period. Green: Dropped because no neighbors found within 80 km radius, or because of singleton country. Black: Preserved, i.e., balanced and consecutive with at least one neighbor each and at least two cells per country. Number of years: 21. Number of preserved cells: 24,184.

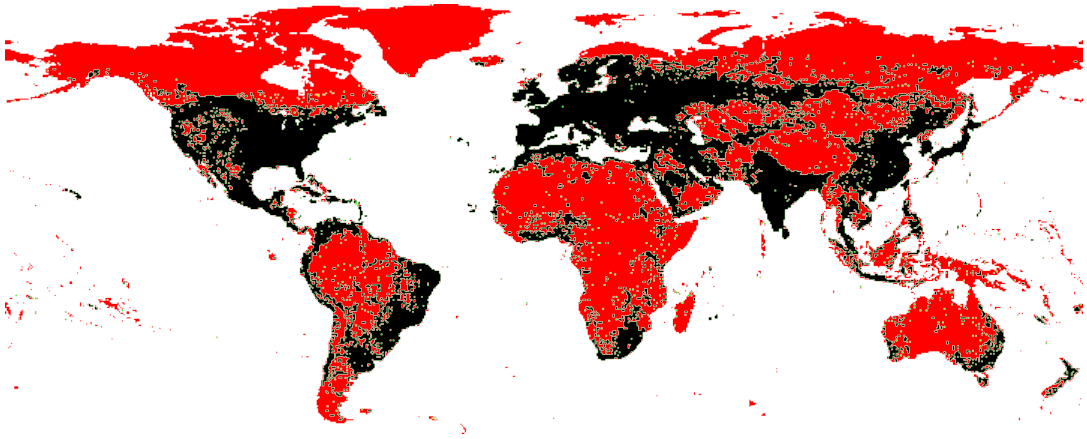

Figure A8: Global distribution of grid cells preserved in balanced panel. Physical indicators used for balancing: Temperature. Red: Dropped because of zero absolute light emission in at least one period and because of missing values in the physical intensity measure. Yellow: Dropped because of zero population in at least one period. Green: Dropped because no neighbors found within 80 km radius, or because of singleton country. Black: Preserved, i.e., balanced and consecutive with at least one neighbor each and at least two cells per country. Number of years: 21. Number of preserved cells: 24,097.

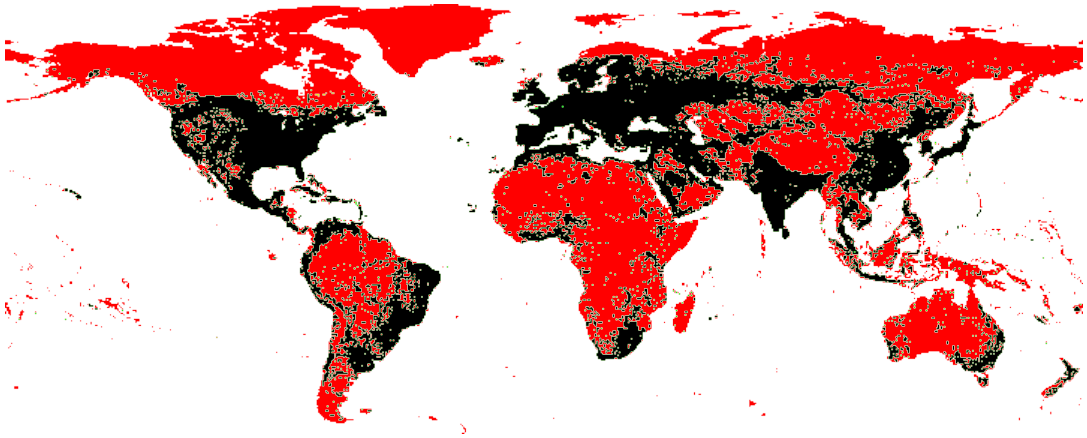

Figure A9: Global distribution of grid cells preserved in balanced panel. Physical indicators used for balancing: Precipitation. Red: Dropped because of zero absolute light emission in at least one period and because of missing values in the physical intensity measure. Yellow: Dropped because of zero population in at least one period. Green: Dropped because no neighbors found within 80 km radius, or because of singleton country. Black: Preserved, i.e., balanced and consecutive with at least one neighbor each and at least two cells per country. Number of years: 21. Number of preserved cells: 23,906.

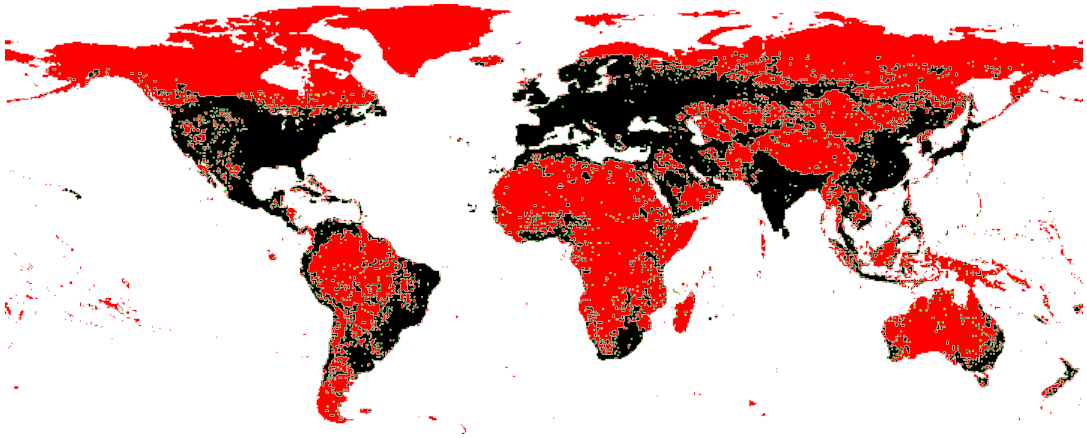

Figure A10: Global distribution of grid cells preserved in balanced panel. Physical indicators used for balancing: Drought. Red: Dropped because of zero absolute light emission in at least one period and because of missing values in the physical intensity measure. Yellow: Dropped because of zero population in at least one period. Green: Dropped because no neighbors found within 80 km radius, or because of singleton country. Black: Preserved, i.e., balanced and consecutive with at least one neighbor each and at least two cells per country. Number of years: 21. Number of preserved cells: 22,294.

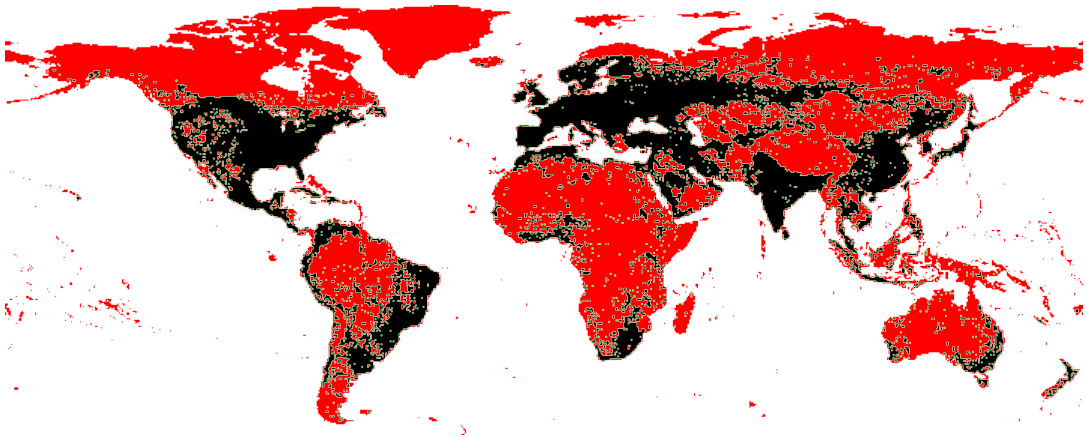

A.4. Rural/Urban Classification

To test the hypothesis that the observed negative spillover effects of droughts are mainly driven by treated non-urban (potentially rural/agricultural) cells that negatively affect nearby urban (or residential) locations, cells must be classified into predominantly urban vs. non-urban ones. For this purpose, the MODIS Landuse Data provided by the FAO for year 2001 is used. This landuse data includes information on the extent of urban or crop areas at a spatial resolution of 15 arc-seconds (i.e., roughly 500 meters), obtained from MODIS satellite imagery using a supervised decision tree classification algorithm with region-specific parameters (Schneider et al., 2009). Urban landuse in particular comprises all human-constructed elements such as buildings and roads, while crop landuse comprises all kinds of cultivated fields. Pixel locations are defined according to the type of landuse they are *dominated* by (i.e., coverage of at least 50% of a given pixel unit). In particular, urban areas follow a defined minimum mapping unit approach, considering only contiguous patches of built-up land that are greater than one square kilometer (i.e., at least four adjacent pixels.). This data is aggregated to $0.5^{\circ}\times0.5^{\circ}$grid cell units by computing the cell level shares of each landuse pixel type.

As a next step, testing the hypothesis requires classifying each cell as either "urban" or "non-urban" in a mutually-exclusive fashion. Due to the presence of snow/ice and other vegetation, crops and urban shares do not sum up to one at the cell level. Moreover, cells with a relatively high share of urban pixels compared to the global distribution may simultaneously also have a relatively high share of rural pixels, and vice versa. Consequently, it is unclear ex-ante, what threshold should be imposed on landuse shares to make a binary distinction.

To solve this classification problem, an off-the-shelve unsupervised machine leaning algorithm provided by Scrucca et al. (2016) is applied, using three input components: The shares of urban, crop, and snow-ice pixels (vs. other vegetation) per cell in year 2001. Using the Bayesian Information Criteria (BIC), the algorithm picks the best fit across a range of classification models. The algorithm chooses an ellipsoidal, equal volume and shape (EEV) Gaussian finite mixture model fitted by expectation-maximization, to classify cells into three categories representing cells that are mostly urban (1,038), mostly non-urban/rural (21,163), and none (93). Thus, about 5% of ever-lit cells in the sample represent mostly urban areas. Figure A11 depicts the classification outcome along the three input-dimensions.

Figure A12 depicts the distributions of key variables of interest for the obtained classes. The top two graphs are dedicated to the distribution of input components used by the

Figure A11: Classification of Rural and Urban Cells in a Gaussian finite mixture model fitted by Expectation-Maximization (EM) algorithm. Ellipsoidal, equal volume and shape (EEV) model with 3 input components: Shares of urban, crop, and snow-ice pixels per cell in year 2001. All input components centered and scaled by their standard deviation for efficiency reasons. Log-Likelihood: 39,242.11, number of observations: 22,294 cells, number of estimated parameters: 23, Bayesian Information Criteria (BIC): 78,253.94, Integrated Complete-data Likelihood (ICL): 77,970.27. Best fit across range of classification models provided by 'mclust 5' R package (Scrucca et al., 2016), using BIC as selection criterion. 21,163 cells classified as rural (red), 1,038 as urban/residential (blue), 93 as none (green).

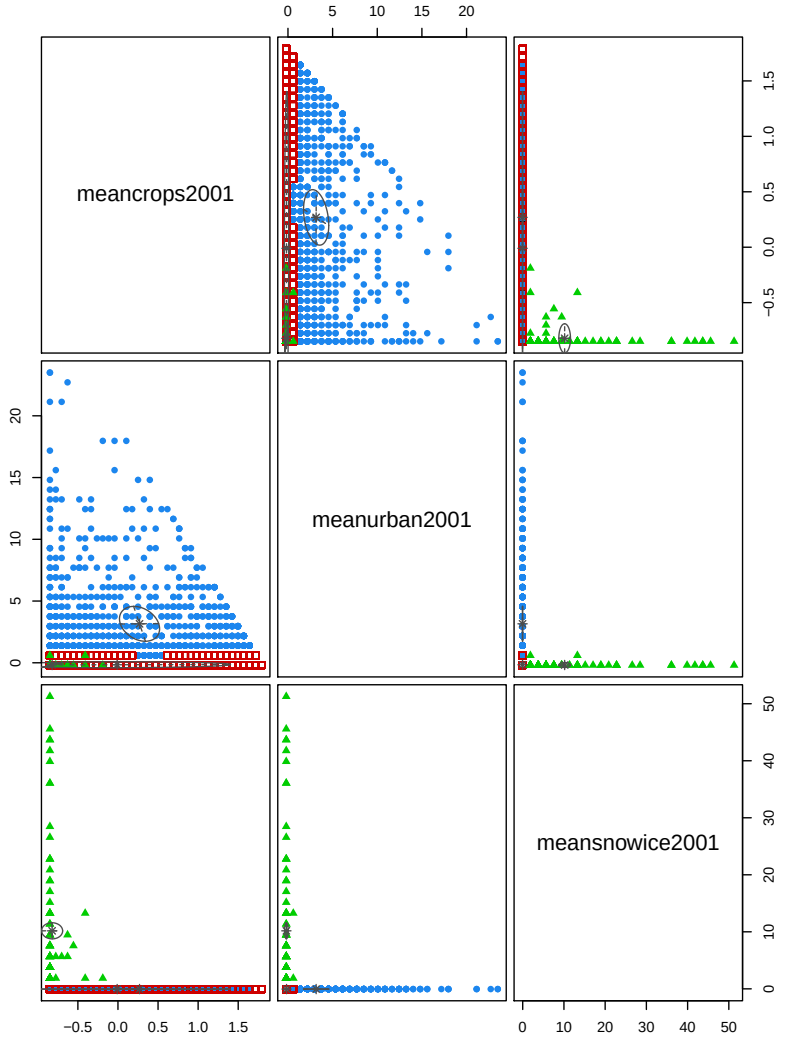

classification algorithm. As it becomes clear, most cells classified as rural have no or only small urban pixel shares. The reverse conclusion is not true however: The graph on the

top right suggests that cells classified as urban may simultaneously have very high crop shares. This observation seems reasonable, given the arbitrary layout of the grid cells combined with the fact that cultivated croplands are often located in the outskirts of urban areas.

The lower two graphs turn to the distributions of the mean night light intensity (left) and of population (right). Neither of these two variables has been used as inputs for classification but are relevant for empirical identification and shall thus serve to asses the class validity. The plots suggest that both the mean night light intensity and the population size are overall higher for urban than for rural cells, which can be considered a reasonable finding.

Finally, to offer a more tractable alternative to the classification with non-supervised learning, a "simple" selection rule is tested, which baldly classifies all cells as urban that have a share of urban pixels which is larger than zero. This approach leads to about twice as many cells being classified as urban, potentially including also those that have only very small urban area. While it is reasonable to assume that about 10% urbanization at a global scale may be too high, results are qualitatively similar.

To decompose the local average treatment and spillover effects of droughts according to cell classification, the following model is estimated:

$$
\begin{aligned}
\Delta \boldsymbol{\ell_t} = {} & \boldsymbol{\ell_{t-1}}\gamma_{t-1} + \boldsymbol{D_t}\boldsymbol{\beta_t^0} + [\boldsymbol{D_t} \times \mathbf{urban}]\,\boldsymbol{\beta_t^1} \\
& + \boldsymbol{W^r_{\text{non-urban}}}\boldsymbol{D_t}\boldsymbol{\beta_t^2} + [\boldsymbol{W^r_{\text{non-urban}}}\boldsymbol{D_t} \times \mathbf{urban}]\,\boldsymbol{\beta_t^3} \\
& + \boldsymbol{W^r_{\text{urban}}}\boldsymbol{D_t}\boldsymbol{\beta_t^4} + [\boldsymbol{W^r_{\text{urban}}}\boldsymbol{D_t} \times \mathbf{urban}]\,\boldsymbol{\beta_t^5} \\
& + \boldsymbol{X_t}\boldsymbol{\delta_t^0} + \boldsymbol{W^r}\boldsymbol{X_t}\boldsymbol{\delta_t^1} + \boldsymbol{\nu} + \boldsymbol{\pi} + \boldsymbol{u_t} \\
\boldsymbol{u_t} = {} & \rho\boldsymbol{W^r}\boldsymbol{u_t} + \boldsymbol{\varepsilon_t}.
\end{aligned}
\tag{5}
$$

W_{urban} and $W_{\text{non-urban}}$ represent mutually exclusive subsets of neighborhoods. Since these subsets potentially have systematic differences in the number of neighbors, spillover-components are standard-normalized to allow direct comparison of coefficient magnitudes. Results for both classifiers (clustering and simple) are summarized in Table A1.

Results suggest that negative spillovers from non-urban to urban cells drive the aggregate spillover, with magnitudes about twice as strong as from non-urban to non-urban ones. This supports the hypothesis that negative drought spillovers are driven by the rural-to-urban channel. Spillovers within pairs of non-urban cells still persist, however, potentially due to residual urban structures in cells classified as non-urban. There is no evidence for spillovers from urban to non-urban cells and only weak spillovers within

Figure A12: Distribution of cell properties across rural/urban clusters.

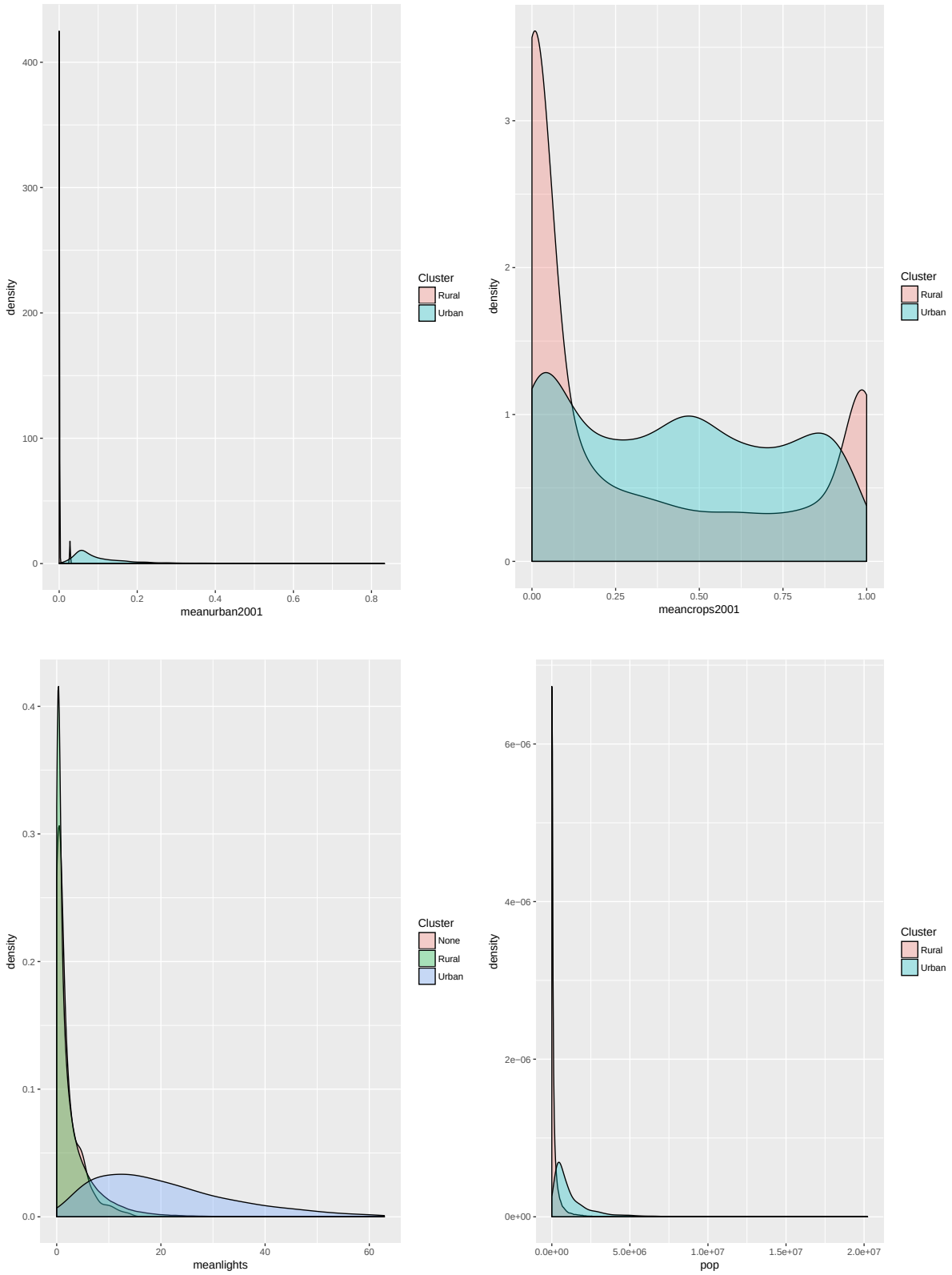

Table A1: Comparison of Drought-Effects Across Rural-Urban Neighborhoods

Dependent Variable: $\Delta \ln(\text{lights}_t)$

			clustering	**simple**
direct effects		**non-urban cells**		
		drought_t	0.0243***	0.0227***
			(0.0039)	(0.0040)
		drought_{t-1}	−0.0046	−0.0038
			(0.0039)	(0.0039)
		urban cells		
		$\text{drought}_t \times \text{urban}$	0.0593***	0.0463***
			(0.0172)	(0.0123)
		$\text{drought}_{t-1} \times \text{urban}$	−0.0289*	−0.0204*
			(0.0172)	(0.0123)
spillover effects	**from non-urban cells**	**to non-urban cells**		
		$W_{\text{non-urban}} \cdot \text{drought}_t$	−0.0080***	−0.0079***
			(0.0015)	(0.0015)
		$W_{\text{non-urban}} \cdot \text{drought}_{t-1}$	−0.0004	−0.0006
			(0.0015)	(0.0015)
		to urban cells		
		$W_{\text{non-urban}} \cdot \text{drought}_t \times \text{urban}$	−0.0094*	−0.0062*
			(0.0051)	(0.0036)
		$W_{\text{non-urban}} \cdot \text{drought}_{t-1} \times \text{urban}$	0.0046	0.0037
			(0.0051)	(0.0036)
	from urban cells	**to non-urban cells**		
		$W_{\text{urban}} \cdot \text{drought}_t$	−0.0012	−0.0004
			(0.0011)	(0.0011)
		$W_{\text{urban}} \cdot \text{drought}_{t-1}$	−0.0005	−0.0005
			(0.0011)	(0.0011)
		to urban cells		
		$W_{\text{urban}} \cdot \text{drought}_t \times \text{urban}$	−0.0042**	−0.0050***
			(0.0019)	(0.0019)
		$W_{\text{urban}} \cdot \text{drought}_{t-1} \times \text{urban}$	0.0034*	0.0025
			(0.0019)	(0.0019)
		controls		
		$\ln(\text{pop}_t)$	0.0276***	0.0276***
			(0.0014)	(0.0014)
		$W \cdot \ln(\text{pop}_t)$	0.0115***	0.0115***
			(0.0006)	(0.0006)
		$\ln(\text{lights}_{t-1})$	−0.4329***	−0.4329***
			(0.0011)	(0.0011)
		ρ	0.0676***	0.0676***
			(0.0001)	(0.0000)
		Observations	468,174	468,174

Note: ***, **, * denote significance at the 1%, 5% and 10% level. All specifications are SDEM and are estimated by Maximum Likelihood. Standard errors in parentheses. Cell and year fixed effects included but not reported. Spatial radius is r=80 km. Yearly disaster intensities reflect time-weighted rolling averages over 12 subsequent monthly observations. W_{urban} and $W_{\text{non-urban}}$ represent mutually exclusive subsets of neighborhoods. Spillover-Components standard-normalized to allow comparison across subsets within regressions.

urban neighborhoods. Finally, the positive direct effect is nearly three times as large in urban cells compared to non-urban ones. Notably also, the relevant spillover effects from non-urban to urban cells are about a third higher with the machine-learning clustering approach than if the simple classification rule is used. This suggests that the distinction between urban and non-urban cells provided by machine-learning may be more precise but is not exclusively driving the qualitative findings.

B. Supplementary Appendix

B.1. Descriptive Statistics

Table A2: Summary Statistics

statistic	n	mean	st. dev.	min	max
Δ ln(lights)	507,864	0.045	0.392	−8.246	8.217
Δ ln(lights NTC)	468,111	0.046	0.394	−8.139	8.109
Δ ln(lights<=DN55)	507,528	0.048	0.402	−0.030	8.002
Δ ln(lights>=DN3)	507,024	0.045	0.397	−8.246	8.217
Δ ln(lights>=DN8)	390,957	0.045	0.483	−8.311	8.424
ln(lights)	507,864	0.264	1.724	−7.090	4.142
ln(lights NTC)	468,111	0.135	1.672	−7.090	4.093
ln(pop_t)	507,864	10.639	2.165	−14.390	16.822
time-weighted physical intensities					
wind	507,864	20.766	4.486	5.478	46.528
cold	506,037	0.412	0.089	0.000	1.271
precip.	502,026	0.385	0.151	0.000	1.697
drought	468,174	0.387	0.242	0.000	2.305
earthq.	507,864	0.121	0.395	−0.189	5.002
simple mean of yearly physical intensities					
wind	507,864	20.735	4.552	4.957	48.036
cold	506,037	0.410	0.093	0.000	1.372
precip.	502,026	0.386	0.182	0.000	1.841
drought	468,174	0.386	0.277	0.000	2.322
earthq.	507,864	0.120	0.405	−0.317	5.342

Figure A13: Specification of World Regions

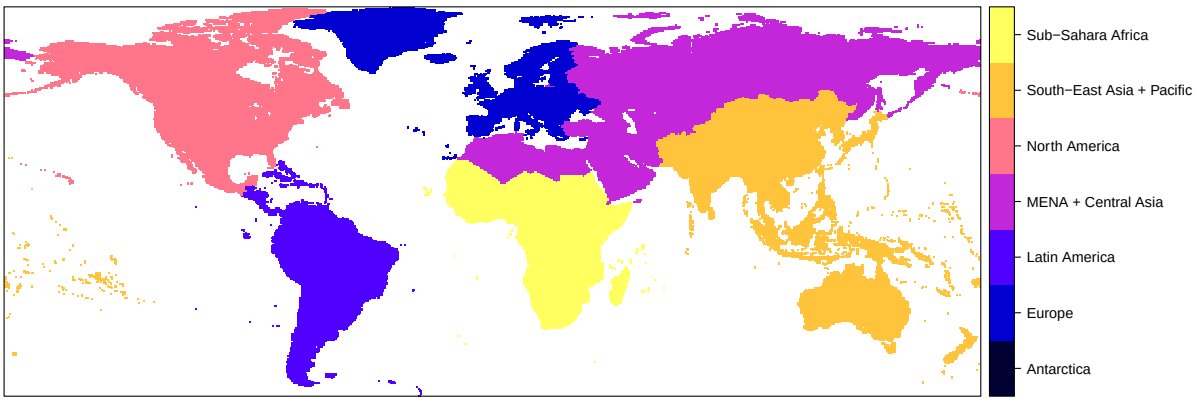

Table A3: Summary Statistics of Satellite-Years for Night-time Lights

Satellite-Year	**DN**							**Cloud-Free Nights**
	0	**1–2**	**3–8**	**9–15**	**16–25**	**26–62**	**63**	**(Mean)**
F101992	84.97%	0.00%	4.00%	1.89%	0.73%	0.85%	0.09%	15.2
F101993	86.34%	0.00%	6.19%	1.65%	0.70%	0.86%	0.00%	31.2
F101994	86.39%	0.00%	6.21%	1.58%	0.69%	0.89%	0.10%	14.7
F121995	84.97%	0.00%	6.26%	1.92%	0.84%	1.08%	0.10%	40.9
F121996	84.79%	0.00%	6.58%	1.82%	0.82%	1.04%	0.09%	40.2
F121997	84.81%	0.00%	5.90%	1.99%	0.85%	1.10%	0.11%	36.3
F121998	82.93%	0.00%	6.01%	2.25%	0.93%	1.18%	0.12%	40.2
F141999	78.35%	0.03%	7.65%	1.45%	0.66%	0.89%	0.08%	37.1
F152000	84.64%	0.00%	7.19%	2.31%	0.92%	1.15%	0.11%	48.7
F152001	81.82%	0.00%	7.49%	2.11%	0.89%	1.15%	0.09%	47.1
F152002	84.02%	0.00%	7.52%	2.19%	0.91%	1.19%	0.09%	53.4
F152003	82.19%	0.19%	8.24%	1.30%	0.63%	0.86%	0.06%	45.8
F152004	84.56%	0.52%	8.57%	1.27%	0.62%	0.89%	0.05%	53.9
F152005	83.91%	0.61%	8.90%	1.37%	0.69%	0.95%	0.06%	59.4
F152006	84.23%	0.56%	8.63%	1.36%	0.67%	0.96%	0.06%	51.6
F162007	84.16%	0.00%	8.16%	1.99%	0.87%	1.20%	0.09%	53.7
F162008	84.32%	0.00%	8.08%	1.92%	0.86%	1.19%	0.10%	47.4
F162009	85.55%	0.00%	6.74%	1.90%	0.87%	1.17%	0.12%	32.0
F182010	83.11%	0.00%	6.43%	3.39%	1.47%	1.87%	0.18%	54.6
F182011	83.56%	0.00%	7.85%	2.44%	1.06%	1.44%	0.14%	54.6
F182012	84.25%	0.00%	6.06%	2.89%	1.20%	1.59%	0.17%	49.4
F182013	84.61%	0.00%	6.16%	2.83%	1.16%	1.57%	0.16%	58.8

Note: Summary statistics are provided for post-cleaning night light satellite-years. Light pixels are considered only on-land, not in gas-flaring zones and in vicinity of volcanoes (see Data Section). Exception: The mean number of cloud-free nights is constructed using the raw data product, as downloaded from NOAA.

Table A4: Lights to GDP Growth Rate Elasticity

Dependent Variable:	**ln(GDP in const. LCU)**		**ln(pop density)**	
ln(light)	0.348***	0.369***		0.097***
	(0.092)	(0.069)		(0.015)
ln(GDP in const. LCU)			0.132***	
			(0.031)	
adj. R^2	0.999	0.998	0.997	0.997
within R^2	0.240	0.273	0.073	0.080
N	3229	4167	4156	4156

Note: ***, **, * denote significance at the 1%, 5% and 10% level. All models use panel OLS. Standard errors (in parentheses) are robust to heteroskedasticity. Country and year fixed effects included but not reported. Years 1992-2008 in first column, 1992-2013 in remaining columns. 197 countries in sample.

Table A5: Test for Residual Spatial Autocorrelation

Global Moran's *I* Test for regression residuals of SLX model

	wind	**precip.**	**drought**	**cold**
Sample Estimates				
Observed Moran's I	0.4466	0.4496	0.4530	0.4459
Expected Moran's I	−0.0001	−0.0001	−0.0001	−0.0001
	0.0000	0.0000	0.0000	0.0000
Test Statistics				
Moran's I stat. s.d.	596.16	596.66	579.01	594.28
Two-sided p-value	2.2e-16	2.2e-16	2.2e-16	2.2e-16

Note: Global Moran's I Test for spatial autocorrelation in the residuals of estimated linear SLX models, compare column (3) of tables A6–A8. The Null Hypothesis of no residual spatial autocorrelation (RSA) is overwhelmingly rejected. Observed Moran's I are positive throughout, suggesting positive RSA (i.e., spatial clustering).

Figure A14: Kernel Densities of Monthly Physical Intensities

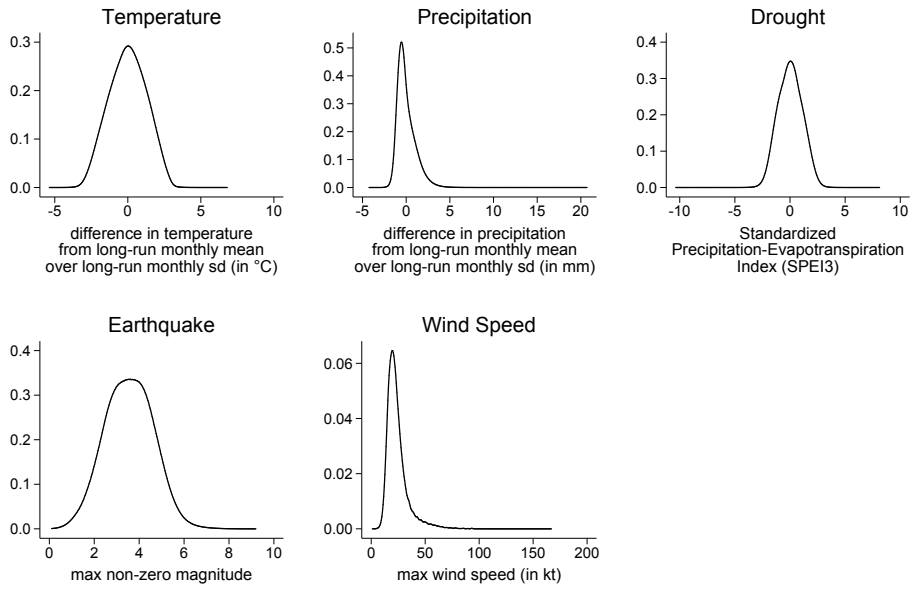

Figure A15: Kernel Densities of Monthly Temperature and Precipitation (raw data)

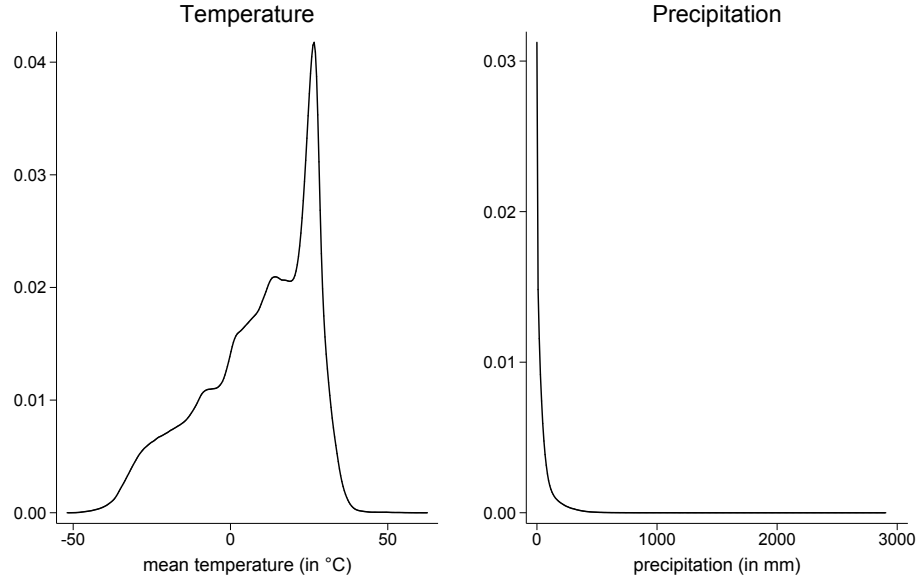

B.2. Regression Tables

Table A6: Model Buildup: Impact of Droughts on Light Growth

Dependent Variable: $\Delta \ln(\text{lights}_t)$

	(1)	(2)	(3)	(4)
drought_t	−0.0229***	0.0262***	0.0345***	0.0083*
	(0.0021)	(0.0055)	(0.0057)	(0.0048)
drought_{t-1}			−0.0296***	0.0005
			(0.0058)	(0.0047)
$W \cdot \text{drought}_t$		−0.0080***	−0.0099***	−0.0044***
		(0.0008)	(0.0008)	(0.0009)
$W \cdot \text{drought}_{t-1}$			0.0073***	0.0010
			(0.0008)	(0.0009)
$\ln(\text{pop}_t)$	0.0432***	0.0267***	0.0266***	0.0276***
	(0.0030)	(0.0029)	(0.0029)	(0.0014)
$W \cdot \ln(\text{pop}_t)$		0.0149***	0.0149***	0.0115
		(0.0009)	(0.0009)	(0.0006)
$\ln(\text{lights}_{t-1})$	−0.4054***	−0.4086***	−0.4084***	−0.4329***
	(0.0033)	(0.0033)	(0.0033)	(0.0011)
ρ				0.676***
				(0.0000)
Method	OLS	SLX	SLX	SDEM
Observations	468,174	468,174	468,174	468,174

Note: ***, **, * denote significance at the 1%, 5% and 10% level. Specifications (1), (2), and (3) are estimated by panel OLS, (4) is estimated by Maximum Likelihood. Standard errors (in parentheses) allow for heteroskedasticity and clustering at the cell level in specifications (1), (2), and (3). Cell and year fixed effects included but not reported. Spatial radius is r=80 km. Yearly disaster intensities reflect time-weighted rolling averages over 12 subsequent monthly observations.

Table A7: Model Buildup: Impact of Cold Waves on Light Growth

Dependent Variable: $\Delta \ln(\text{lights}_t)$

	(1)	(2)	(3)	(4)
cold_t	0.0134**	−0.1765***	−0.1227***	−0.0762***
	(0.0068)	(0.0184)	(0.0194)	(0.0153)
cold_{t-1}			−0.0293*	−0.0326**
			(0.0176)	(0.0149)
$W \cdot \text{cold}_t$		0.0323***	0.0307***	0.0218***
		(0.0025)	(0.0026)	(0.0027)
$W \cdot \text{cold}_{t-1}$			−0.0229***	−0.0195***
			(0.0024)	(0.0026)
$\ln(\text{pop}_t)$	0.0409***	0.0236***	0.0233***	0.0244***
	(0.0028)	(0.0027)	(0.0027)	(0.0013)
$W \cdot \ln(\text{pop}_t)$		0.0148***	0.0142***	0.0106***
		(0.0008)	(0.0008)	(0.0006)
$\ln(\text{lights}_{t-1})$	−0.4097***	−0.4141***	−0.4138***	−0.4379***
	(0.0032)	(0.0032)	(0.0032)	(0.0011)
ρ				0.0672***
				(0.0000)
Method	OLS	SLX	SLX	SDEM
Observations	506,394	506,394	506,037	506,037

Note: ***, **, * denote significance at the 1%, 5% and 10% level. Specifications (1), (2), and (3) are estimated by panel OLS, (4) is estimated by Maximum Likelihood. Standard errors (in parentheses) allow for heteroskedasticity and clustering at the cell level in specifications (1), (2), and (3). Cell and year fixed effects included but not reported. Spatial radius is r=80 km. Yearly disaster intensities reflect time-weighted rolling averages over 12 subsequent monthly observations.

Table A8: Model Buildup: Impact of Earthquakes on Light Growth

Dependent Variable: $\Delta \ln(\text{lights}_t)$

	(1)	(2)	(3)	(4)
$\text{earthq}_{\cdot t}$	0.0107***	0.0055**	0.0038	0.0044**
	(0.0018)	(0.0022)	(0.0023)	(0.0022)
$\text{earthq}_{\cdot t-1}$			0.0032	0.0011
			(0.0024)	(0.0022)
$W \cdot \text{earthq}_{\cdot t}$		0.0019***	0.0008	0.0005
		(0.0005)	(0.0006)	(0.0008)
$W \cdot \text{earthq}_{\cdot t-1}$			0.0018***	0.0015*
			(0.0007)	(0.0008)
$\ln(\text{pop}_t)$	0.0406***	0.0243***	0.0243***	0.0251***
	(0.0028)	(0.0027)	(0.0027)	(0.0013)
$W \cdot \ln(\text{pop}_t)$		0.0148***	0.0147***	0.0111***
		(0.0008)	(0.0008)	(0.0006)
$\ln(\text{lights}_{t-1})$	−0.4101***	−0.4134***	−0.4134***	−0.4378***
	(0.0032)	(0.0032)	(0.0032)	(0.0011)
ρ				0.672***
				(0.0000)
Method	OLS	SLX	SLX	SDEM
Observations	507,864	507,864	507,864	507,864

Note: ***, **, * denote significance at the 1%, 5% and 10% level. Specifications (1), (2), and (3) are estimated by panel OLS, (4) is estimated by Maximum Likelihood. Standard errors (in parentheses) allow for heteroskedasticity and clustering at the cell level in specifications (1), (2), and (3). Cell and year fixed effects included but not reported. Spatial radius is r=80 km. Yearly disaster intensities reflect time-weighted rolling averages over 12 subsequent monthly observations.

Table A9: Sensitivity to Top-Coding: Excluding Top-Coded Pixels

Dependent Variable: $\Delta \ln(\text{lights}_t)$

	wind	**precip.**	**drought**	**cold**
disaster_t	−0.0019**	−0.0329***	0.0091*	−0.0752***
	(0.0009)	(0.0070)	(0.0048)	(0.0152)
disaster_{t-1}	−0.0090***	0.0222***	0.0012	−0.0318**
	(0.0009)	(0.0069)	(0.0048)	(0.0149)
$W \cdot \text{disaster}_t$	0.0000	0.0052***	−0.0046***	0.0219***
	(0.0002)	(0.0013)	(0.0009)	(0.0027)
$W \cdot \text{disaster}_{t-1}$	0.0008***	−0.0023*	0.0011	−0.0200***
	(0.0002)	(0.0013)	(0.0009)	(0.0027)
$\ln(\text{pop}_t)$	0.0276***	0.0286***	0.0302***	0.0273***
	(0.0013)	(0.0013)	(0.0014)	(0.0013)
$W \cdot \ln(\text{pop}_t)$	0.0113***	0.0117***	0.0119***	0.0110***
	(0.0006)	(0.0006)	(0.0006)	(0.0006)
$\ln(\text{lights}_{t-1})$	−0.4381***	−0.4360***	−0.4321***	−0.4373***
	(0.0011)	(0.0011)	(0.0011)	(0.0011)
ρ	0.0672***	0.0672***	0.0676***	0.0672***
	(0.0000)	(0.0000)	(0.0000)	(0.0000)
Observations	507,780	501,942	468,111	505,953

Note: ***, **, * denote significance at the 1%, 5% and 10% level. All specifications are SDEM and are estimated by Maximum Likelihood. Standard errors in parentheses. Cell and year fixed effects included but not reported. Spatial radius is r=80 km. Yearly disaster intensities reflect time-weighted rolling averages over 12 subsequent monthly observations. Dependent variable excludes top-coded pixels.

Table A10: Sensitivity to top-coding: masking all >DN55 pixels

Dependent Variable: $\Delta \ln(\text{lights}_t)$

	wind	**precip.**	**drought**	**cold**
disaster_t	−0.0019**	−0.0359***	0.0104**	−0.0784***
	(0.0009)	(0.0070)	(0.0048)	(0.0153)
disaster_{t-1}	−0.0091***	0.0227***	0.0024	−0.0275*
	(0.0002)	(0.0069)	(0.0047)	(0.0150)
$W \cdot \text{disaster}_t$	0.0000	0.0056***	−0.0049***	0.0229***
	(0.0002)	(0.0013)	(0.0009)	(0.0027)
$W \cdot \text{disaster}_{t-1}$	0.0008***	−0.0026**	0.0012	−0.0209***
	(0.0002)	(0.0013)	(0.0009)	(0.0027)
$\ln(\text{pop}_t)$	0.0301***	0.0311***	0.0326***	0.0299***
	(0.0013)	(0.0013)	(0.0014)	(0.0013)
$W \cdot \ln(\text{pop}_t)$	0.0114***	0.0118***	0.0120***	0.0111***
	(0.0006)	(0.0006)	(0.0006)	(0.0006)
$\ln(\text{lights}_{t-1})$	−0.4360***	−0.4338***	−0.4300***	−0.4352***
	(0.0011)	(0.0011)	(0.0011)	(0.0011)
ρ	0.0672***	0.0672***	0.0676***	0.0676***
	(0.0000)	(0.0000)	(0.0000)	(0.0000)
Observations	507,528	501,795	468,048	505,764

Note: ***, **, * denote significance at the 1%, 5% and 10% level. All specifications are SDEM and are estimated by Maximum Likelihood. Standard errors in parentheses. Cell and year fixed effects included but not reported. Spatial radius is r=80 km. Yearly disaster intensities reflect time-weighted rolling averages over 12 subsequent monthly observations.

Table A11: Sensitivity to Bottom-Coding: Setting Pixels <DN8 to Zero

Dependent Variable: $\Delta \ln(\text{lights}_t)$

	wind	**precip.**	**drought**	**cold**
disaster_t	0.0009	−0.0145*	−0.0032	−0.0208
	(0.0011)	(0.0084)	(0.0058)	(0.0186)
disaster_{t-1}	−0.0093***	0.0215***	0.0063	−0.1174***
	(0.0011)	(0.0083)	(0.0058)	(0.0183)
$W \cdot \text{disaster}_t$	−0.0011***	0.0066***	−0.0040***	0.0172***
	(0.0002)	(0.0017)	(0.0012)	(0.0035)
$W \cdot \text{disaster}_{t-1}$	0.0004**	−0.0031*	−0.0015	−0.0206***
	(0.0002)	(0.0017)	(0.0012)	(0.0035)
$\ln(\text{pop}_t)$	0.0201***	0.0204***	0.0236***	0.0188***
	(0.0019)	(0.0019)	(0.0020)	(0.0019)
$W \cdot \ln(\text{pop}_t)$	0.0158***	0.0161***	0.0168***	0.0150***
	(0.0009)	(0.0009)	(0.0009)	(0.0009)
$\ln(\text{lights}_{t-1})$	−0.3756***	−0.3738***	−0.3700***	−0.3742***
	(0.0012)	(0.0012)	(0.0012)	(0.0012)
ρ	0.0679***	0.0680***	0.0684***	0.0679***
	(0.0000)	(0.0000)	(0.0000)	(0.0000)
Observations	390,957	388,227	362,607	390,201

Note: ***, **, * denote significance at the 1%, 5% and 10% level. All specifications are SDEM and are estimated by Maximum Likelihood. Standard errors in parentheses. Cell and year fixed effects included but not reported. Spatial radius is r=80 km. Yearly disaster intensities reflect time-weighted rolling averages over 12 subsequent monthly observations.

Table A12: Sensitivity to bottom-coding: setting pixels <DN3 to zero

Dependent Variable: $\Delta \ln(\text{lights}_t)$

	wind	**precip.**	**drought**	**cold**
disaster_t	−0.0007	−0.0265***	0.0082*	−0.0852***
	(0.0009)	(0.0070)	(0.0048)	(0.0154)
disaster_{t-1}	−0.0106***	0.0290***	0.0015	−0.0291*
	(0.0009)	−0.0069	(0.0048)	(0.0150)
$W \cdot \text{disaster}_t$	−0.0001	0.0042***	−0.0041***	0.0242***
	(0.0002)	(0.0013)	(0.0009)	(0.0027)
$W \cdot \text{disaster}_{t-1}$	0.0010***	−0.0022*	0.0007	−0.0217***
	(0.0002)	(0.0013)	(0.0009)	(0.0027)
$\ln(\text{pop}_t)$	0.0265***	0.0275***	0.0296***	0.0262***
	(0.0013)	(0.0013)	(0.0014)	(0.0013)
$W \cdot \ln(\text{pop}_t)$	0.0108***	0.0112***	0.0116***	0.0105***
	(0.0006)	(0.0006)	(0.0006)	(0.0006)
$\ln(\text{lights}_{t-1})$	−0.4395***	−0.4376***	−0.4338***	−0.4388***
	(0.0011)	(0.0011)	(0.0011)	(0.0011)
ρ	0.0672***	0.0672***	0.0676***	0.0672***
	(0.0000)	(0.0000)	(0.0000)	(0.0000)
Observations	507,024	501,228	467,460	505,197

Note: ***, **, * denote significance at the 1%, 5% and 10% level. All specifications are SDEM and are estimated by Maximum Likelihood. Standard errors in parentheses. Cell and year fixed effects included but not reported. Spatial radius is r=80 km. Yearly disaster intensities reflect time-weighted rolling averages over 12 subsequent monthly observations.

Table A13: Sensitivity of Baseline Results to Radius r=160km

Dependent Variable: $\Delta \ln(\text{lights}_t)$

	wind	**precip.**	**drought**	**cold**
disaster_t	−0.0016**	−0.0249***	0.0125***	−0.0849***
	(0.0007)	(0.0057)	(0.0041)	(0.0136)
disaster_{t-1}	−0.0052***	0.0158***	−0.0075*	−0.0129
	(0.0007)	(0.0057)	(0.0040)	(0.0133)
$W \cdot \text{disaster}_t$	0.0000	0.0008**	−0.0015***	0.0061***
	(0.0000)	(0.0004)	(0.0003)	(0.0009)
$W \cdot \text{disaster}_{t-1}$	0.0001*	0.0000	0.0005*	−0.0060***
	(0.0000)	(0.0004)	(0.0003)	(0.0008)
$\ln(\text{pop}_t)$	0.0245***	0.0252***	0.0264***	0.0240***
	(0.0013)	(0.0013)	(0.0014)	(0.0013)
$W \cdot \ln(\text{pop}_t)$	0.0057***	0.0059***	0.0061***	0.0055***
	(0.0003)	(0.0003)	(0.0003)	(0.0003)
$\ln(\text{lights}_{t-1})$	−0.4375***	−0.4360***	−0.4328***	−0.4371***
	(0.0011)	(0.0011)	(0.0011)	(0.0011)
ρ	0.0220***	0.0221***	0.0226***	0.0220***
	(0.0000)	(0.0000)	(0.0000)	(0.0000)
Observations	515,130	509,166	475,083	513,282

Note: ***, **, * denote significance at the 1%, 5% and 10% level. All specifications are SDEM and are estimated by Maximum Likelihood. Standard errors in parentheses. Cell and year fixed effects included but not reported. Spatial radius is r=160 km. Yearly disaster intensities reflect time-weighted rolling averages over 12 subsequent monthly observations.

Table A14: Sensitivity of Baseline Results to Time Varying Country Characteristics

Dependent Variable: $\Delta \ln(\text{lights}_t)$

	wind	**precip.**	**drought**	**cold**
disaster_t	0.0004	−0.0312***	0.0062	−0.0360**
	(0.0010)	(0.0070)	(0.0049)	(0.0179)
disaster_{t-1}	−0.0049***	0.0117*	0.0009	−0.0390**
	(0.0010)	(0.0069)	(0.0049)	(0.0175)
$W \cdot \text{disaster}_t$	0.0003**	0.0043***	−0.0041***	0.0165***
	(0.0002)	(0.0013)	(0.0009)	(0.0029)
$W \cdot \text{disaster}_{t-1}$	0.0009***	−0.0022*	0.0017*	−0.0144***
	(0.0002)	(0.0013)	(0.0009)	(0.0028)
$\ln(\text{pop}_t)$	0.0140***	0.0145***	0.0158***	0.0140***
	(0.0013)	(0.0013)	(0.0014)	(0.0013)
$W \cdot \ln(\text{pop}_t)$	0.0040***	0.0041***	0.0044***	0.0039***
	(0.0006)	(0.0006)	(0.0006)	(0.0006)
$\ln(\text{lights}_{t-1})$	−0.4768***	−0.4759***	−0.4728***	−0.4764***
	(0.0011)	(0.0011)	(0.0012)	(0.0011)
ρ	0.0671***	0.0671***	0.0068***	0.0671***
	(0.0000)	(0.0000)	(0.0000)	(0.0000)
Observations	507,864	502,026	468,174	506,037

Note: ***, **, * denote significance at the 1%, 5% and 10% level. All specifications are SDEM and are estimated by Maximum Likelihood. Standard errors in parentheses. Cell and country-year fixed effects (with nested year fixed effects) included but not reported. Spatial radius is r=80 km. Yearly disaster intensities reflect time-weighted rolling averages over 12 subsequent monthly observations.

Table A15: Sensitivity of Baseline to Simple Annual Mean of Disasters

Dependent Variable: $\Delta \ln(\text{lights}_t)$

	wind	**precip.**	**drought**	**cold**
disaster_t	−0.0032***	−0.0289***	0.0243***	−0.0613***
	(0.0007)	(0.0055)	(0.0039)	(0.0137)
disaster_{t-1}	−0.0064***	0.0011	−0.0060	−0.0540***
	(0.007)	(0.0055)	(0.0038)	(0.0133)
$W \cdot \text{disaster}_t$	−0.0002	0.0018*	−0.0037***	0.0337***
	(0.0001)	(0.0010)	(0.0007)	(0.0025)
$W \cdot \text{disaster}_{t-1}$	0.0008***	0.0030***	0.0000	−0.0504***
	(0.0001)	(0.0010)	(0.0007)	(0.0019)
$\ln(\text{pop}_t)$	0.0247***	0.0257***	0.0276***	0.0245***
	(0.0013)	(0.0013)	(0.0014)	(0.0013)
$W \cdot \ln(\text{pop}_t)$	0.0109***	0.0113***	0.0115***	0.0107***
	(0.0006)	(0.0006)	(0.0006)	(0.0006)
$\ln(\text{lights}_{t-1})$	−0.4385***	−0.4367***	−0.4329***	−0.4376***
	(0.0011)	(0.0011)	(0.0011)	(0.0011)
ρ	0.0672***	0.0672***	0.676***	0.0672***
	(0.0000)	(0.0000)	(0.0000)	(0.0000)
Observations	507,864	502,026	468,174	506,037

Note: ***, **, * denote significance at the 1%, 5% and 10% level. All specifications are SDEM and are estimated by Maximum Likelihood. Standard errors in parentheses. Cell and year fixed effects included but not reported. Spatial radius is r=80 km. Yearly disaster intensities reflect non-weighted mean over all monthly observations within a year.

Table A16: Sensitivity of Baseline Results to Global Spillovers

Dependent Variable: $\Delta \ln(\text{lights}_t)$

	wind	**precip.**	**drought**	**cold**
disaster_t	−0.0046***	−0.0279***	−0.0016	−0.0974***
	(0.0007)	(0.0060)	(0.0041)	(0.0122)
	[−0.0044]	[−0.0259]	[−0.0029]	[−0.0794]
disaster_{t-1}	−0.0095***	0.0198***	0.0017	−0.0858***
	(0.0007)	(0.0059)	(0.0041)	(0.0119)
	[−0.0093]	[0.0189]	[0.0017]	[−0.0908]
$W \cdot \text{disaster}_t$	0.0005***	0.0037***	−0.0010*	0.0217***
	(0.0001)	(0.0009)	(0.0006)	(0.0017)
	[0.0000]	[0.0001]	[−0.0001]	[0.0010]
$W \cdot \text{disaster}_{t-1}$	0.0008***	−0.0021**	−0.0001	0.0015
	(0.0001)	(0.0009)	(0.0006)	(0.0017)
	[0.0000]	[−0.0001]	[0.0000]	[−0.0003]
$\ln(\text{pop}_t)$	0.0228***	0.0242***	0.0256***	0.0225***
	(0.0014)	(0.0014)	(0.0015)	(0.0014)
	[0.0383]	[0.0397]	[0.0412]	[0.0383]
$W \cdot \ln(\text{pop}_t)$	0.0116***	0.0122***	0.0121***	0.0118***
	(0.0004)	(0.0004)	(0.0005)	(0.0004)
	[0.0009]	[0.0009]	[0.0009]	[0.0009]
$\ln(\text{lights}_{t-1})$	−0.3300***	−0.3270***	−0.3232***	−0.3289***
	(0.0009)	(0.0009)	(0.0009)	(0.0009)
λ	0.0671***	0.0671***	0.0675***	0.0671***
	(0.0000)	(0.0000)	(0.0000)	(0.0000)
Observations	508,158	502,320	468,384	506,394

Note: ***, **, * denote significance at the 1%, 5% and 10% level. All specifications are SDM and are estimated by Maximum Likelihood. Standard errors in parentheses. Average effects translated with spatial multiplier in square brackets. Cell and year fixed effects included but not reported. Spatial radius is r=80 km. Yearly disaster intensities reflect time-weighted rolling averages over 12 subsequent monthly observations.

Table A17: Spatial Error HAC Model following Hsiang (2010)

Dependent Variable: $\Delta \ln(\text{lights}_t)$

	wind	**precip.**	**drought**	**cold**
disaster_t	−0.0010	−0.0744***	0.0342***	−0.1219***
	(0.0014)	(0.0112)	(0.0080)	(0.0275)
disaster_{t-1}	−0.0143***	0.0477***	−0.0292***	−0.0301
	(0.0014)	(0.0108)	(0.0079)	(0.0253)
$W \cdot \text{disaster}_t$	−0.0002	0.0137***	−0.0098***	0.0306***
	(0.0002)	(0.0019)	(0.0013)	(0.0043)
$W \cdot \text{disaster}_{t-1}$	0.0015***	−0.0079***	0.0072***	−0.0228***
	(0.0002)	(0.0018)	(0.0013)	(0.0041)
$\ln(\text{pop}_t)$	0.0237***	0.0250***	0.0267***	0.0234***
	(0.0020)	(0.0020)	(0.0021)	(0.0020)
$W \cdot \ln(\text{pop}_t)$	0.0142***	0.0149***	0.0149***	0.0141***
	(0.0011)	(0.0011)	(0.0012)	(0.0011)
$\ln(\text{lights}_{t-1})$	−0.4153***	−0.4123***	−0.4085***	−0.4139***
	(0.0035)	(0.0035)	(0.0037)	(0.0035)
	−0.0018	−0.0052	−0.0058	−0.0033
	(0.0050)	(0.0051)	(0.0053)	(0.0051)
Observations	507,864	502,320	468,384	506,394

Note: ***, **, * denote significance at the 1%, 5% and 10% level. All specifications adapt the Spatial Error HAC Model methods by Conley (1999) as implemented by Hsiang (2010). Standard errors (in parentheses) allow for heteroskedasticity, spatial autocorrelation and temporal autocorrelation over 3 periods. Cell and year fixed effects included but not reported. Spatial radius is r=80 km. Yearly disaster intensities reflect time-weighted rolling averages over 12 subsequent monthly observations.

Table A18: Income Interaction

Dependent Variable: $\Delta \ln(\text{lights}_t)$

	wind		**precip.**		**drought**		**cold**	
	estimate	**combined**	**estimate**	**combined**	**estimate**	**combined**	**estimate**	**combined**
disaster_t	−0.0015		0.0171		−0.0120		0.2442***	
	(0.0016)		(0.0118)		(0.0093)		(0.0389)	
disaster_{t-1}	−0.0042***		0.0249**		0.0081		−0.0680*	
	(0.0015)		(0.0117)		(0.0092)		(0.0384)	
$W \cdot \text{disaster}_t$	−0.0001		0.0015		−0.0020		0.0077	
	(0.0003)		(0.0021)		(0.0016)		(0.0059)	
$W \cdot \text{disaster}_{t-1}$	0.0006**		−0.0040*		0.0029*		−0.0224***	
	(0.0003)		(0.0021)		(0.0016)		(0.0059)	
$\text{disaster}_t \times$ low income	−0.0006	−0.0021*	−0.0705***	−0.0534***	0.0267**	0.0147***	−0.3575***	−0.1133***
	(0.0019)	(0.0011)	(0.0146)	(0.0087)	(0.0108)	(0.0056)	(0.0423)	(0.0169)
$\text{disaster}_{t-1} \times$ low income	−0.0076***	−0.0119***	−0.0057	0.0192**	−0.0092	−0.0010	0.0484	−0.0193
	(0.0019)	(0.0011)	(0.0144)	(0.0085)	(0.0107)	(0.0055)	(0.0416)	(0.0165)
$W \cdot \text{disaster}_t \times$ low income	0.0003	0.0001	0.0049*	0.0064***	−0.0032*	−0.0052***	0.0114*	0.0191***
	(0.0003)	(0.0002)	(0.0026)	(0.0016)	(0.0019)	(0.0011)	(0.0067)	(0.0031)
$W \cdot \text{disaster}_{t-1} \times$ low income	0.0003	0.0009***	0.0033	−0.0007	−0.0029	0.0000	0.0054	−0.0170***
	(0.0003)	(0.0002)	(0.0026)	(0.0016)	(0.0019)	(0.0010)	(0.0066)	(0.0030)
$\ln(\text{pop}_t)$	0.0247***		0.0258***		0.0277***		0.0241***	
	(0.0013)		(0.0013)		(0.0014)		(0.0013))	
$W \cdot \ln(\text{pop}_t)$	0.0109***		0.0112***		0.0115***		0.0103***	
	(0.0006)		(0.0006)		(0.0006)		(0.0006)	
$\ln(\text{lights}_{t-1})$	−0.4386***		−0.4366***		−0.4328***		−0.4382***	
	(0.0011)		(0.0011)		(0.0011)		(0.0011)	
ρ	0.0672***		0.0672***		0.0676***		0.0672***	
	(0.0000)		(0.0000)		(0.0000)		(0.0000)	
Observations	506,142		500,787		467,691		504,525	

Note: ***, **, * denote significance at the 1%, 5% and 10% level. All specifications are SDEM and are estimated by Maximum Likelihood. Standard errors in parentheses. Cell and year fixed effects included but not reported. Spatial radius is r=80 km. Yearly disaster intensities reflect time-weighted rolling averages over 12 subsequent monthly observations.

Table A19: Region: Europe

Dependent Variable: $\Delta \ln(\text{lights}_t)$

	wind	**precip.**	**drought**	**cold**
disaster_t	−0.0034*	0.0116	0.0042	0.0906**
	(0.0018)	(0.0161)	(0.0129)	(0.0442)
disaster_{t-1}	0.0042**	0.0046	0.0011	−0.0858*
	(0.0018)	(0.0160)	(0.0128)	(0.0442)
$W \cdot \text{disaster}_t$	−0.0002	0.0033	−0.0077***	0.0295***
	(0.0003)	(0.0025)	(0.0019)	(0.0057)
$W \cdot \text{disaster}_{t-1}$	0.0005*	0.0016	0.0006	−0.0283***
	(0.0003)	(0.0024)	(0.0019)	(0.0057)
$\ln(\text{pop}_t)$	−0.0002	0.0010	0.0076	−0.0008
	(0.0054)	(0.0055)	(0.0062)	(0.0055)
$W \cdot \ln(\text{pop}_t)$	0.0011	0.0023	0.0042**	0.0011
	(0.0019)	(0.0019)	(0.0021)	(0.0019)
$\ln(\text{lights}_{t-1})$	−0.5916***	−0.5919***	−0.5813***	−0.5918***
	(0.0031)	(0.0032)	(0.0034)	(0.0032)
ρ	0.0673***	0.0673***	0.0677***	0.0673***
	(0.0000)	(0.0000)	(0.0000)	(0.0000)
Observations	70,539	69,447	61,236	70,014

Note: ***, **, * denote significance at the 1%, 5% and 10% level. All specifications are SDEM and are estimated by Maximum Likelihood. Standard errors in parentheses. Cell and year fixed effects included but not reported. Spatial radius is r=80 km. Yearly disaster intensities reflect time-weighted rolling averages over 12 subsequent monthly observations.

Table A20: Region: North America

Dependent Variable: $\Delta \ln(\text{lights}_t)$

	wind	**precip.**	**drought**	**cold**
disaster_t	−0.0076***	0.0026	−0.0245***	0.0256***
	(0.0020)	(0.0132)	(0.0091)	(0.0428)
disaster_{t-1}	−0.0064***	0.0049	0.0049	−0.1636***
	(0.0020)	(0.0130)	(0.0090)	(0.0421)
$W \cdot \text{disaster}_t$	0.0007*	0.0013	0.0021	0.0111
	(0.0004)	(0.0027)	(0.0019)	(0.0073)
$W \cdot \text{disaster}_{t-1}$	0.0011***	−0.0037	0.0045**	0.0022
	(0.0004)	(0.0027)	(0.0019)	(0.0072)
$\ln(\text{pop}_t)$	−0.0016	−0.0026	−0.0022	−0.0025
	(0.0020)	(0.0020)	(0.0021)	(0.0020)
$W \cdot \ln(\text{pop}_t)$	0.0013	0.0012	0.0007	0.0011
	(0.0010)	(0.0010)	(0.0010)	(0.0010)
$\ln(\text{lights}_{t-1})$	−0.5871***	−0.5960***	−0.5796***	−0.5865***
	(0.0027)	(0.0027)	(0.0028)	(0.0027)
ρ	0.0893***	0.0894***	0.0901***	0.0892***
	(0.0004)	(0.0004)	(0.0004)	(0.0004)
Observations	100,653	100,254	94,479	100,485

Note: ***, **, * denote significance at the 1%, 5% and 10% level. All specifications are SDEM and are estimated by Maximum Likelihood. Standard errors in parentheses. Cell and year fixed effects included but not reported. Spatial radius is r=80 km. Yearly disaster intensities reflect time-weighted rolling averages over 12 subsequent monthly observations.

Table A21: Region: Latin America and Caribbean

Dependent Variable: $\Delta \ln(\text{lights}_t)$

	wind	**precip.**	**drought**	**cold**
disaster_t	−0.0048**	−0.0659***	0.0373***	−0.1388***
	(0.0023)	(0.0154)	(0.0103)	(0.0239)
disaster_{t-1}	−0.0064***	0.0483***	−0.0493***	−0.0140
	(0.0023)	(0.0151)	(0.0101)	(0.0238)
$W \cdot \text{disaster}_t$	0.0012**	−0.0022	−0.0008	0.0117**
	(0.0005)	(0.0032)	(0.0022)	(0.0046)
$W \cdot \text{disaster}_{t-1}$	0.0009*	−0.0034	0.0015	0.0086*
	(0.0005)	(0.0032)	(0.0022)	(0.0046)
$\ln(\text{pop}_t)$	0.0336***	0.0378***	0.0393***	0.0339***
	(0.0037)	(0.0038)	(0.0040)	(0.0038)
$W \cdot \ln(\text{pop}_t)$	0.0178***	0.0173***	0.0166***	0.0156***
	(0.0020)	(0.0020)	(0.0021)	(0.0020)
$\ln(\text{lights}_{t-1})$	−0.4516***	−0.4494***	−0.4474***	−0.4506***
	(0.0028)	(0.0028)	(0.0029)	(0.0028)
ρ	0.0788***	0.0785***	0.0784***	0.0788***
	(0.0008)	(0.0008)	(0.0008)	(0.0008)

Note: ***, **, * denote significance at the 1%, 5% and 10% level. All specifications are SDEM and are estimated by Maximum Likelihood. Standard errors in parentheses. Cell and year fixed effects included but not reported. Spatial radius is r=80 km. Yearly disaster intensities reflect time-weighted rolling averages over 12 subsequent monthly observations.

Table A22: Region: Sout-East Asia and Pacific

Dependent Variable: $\Delta \ln(\text{lights}_t)$

	wind	**precip.**	**drought**	**cold**
disaster_t	−0.0032*	−0.0277*	0.0021	0.1020***
	(0.0017)	(0.0161)	(0.0115)	(0.0333)
disaster_{t-1}	−0.0080***	0.0021	0.0349***	0.1289***
	(0.0016)	(0.0159)	(0.0112)	(0.0324)
$W \cdot \text{disaster}_t$	−0.0001	0.0014	−0.0066**	−0.0104
	(0.0004)	(0.0042)	(0.0027)	(0.0080)
$W \cdot \text{disaster}_{t-1}$	0.0001	0.0078*	−0.0047*	−0.0021
	(0.0004)	(0.0042)	(0.0027)	(0.0078)
$\ln(\text{pop}_t)$	0.0378***	0.0388***	0.0443***	0.0378***
	(0.0035)	(0.0035)	(0.0038)	(0.0035)
$W \cdot \ln(\text{pop}_t)$	0.0062***	0.0053**	0.0062***	0.0065***
	(0.0019)	(0.0019)	(0.0021)	(0.0019)
$\ln(\text{lights}_{t-1})$	−0.4179***	−0.4119***	−0.4061***	−0.4166***
	(0.0022)	(0.0022)	(0.0024)	(0.0022)
ρ	0.0962***	0.0966***	0.0970***	0.0963***
	(0.0004)	(0.0004)	(0.0004)	(0.0004)
Observations	112,560	110,523	100,821	112,056

Note: ***, **, * denote significance at the 1%, 5% and 10% level. All specifications are SDEM and are estimated by Maximum Likelihood. Standard errors in parentheses. Cell and year fixed effects included but not reported. Spatial radius is r=80 km. Yearly disaster intensities reflect time-weighted rolling averages over 12 subsequent monthly observations.

Table A23: Region: MENA and Central Asia

Dependent Variable: $\Delta \ln(\text{lights}_t)$

	wind	**precip.**	**drought**	**cold**
disaster_t	0.0061**	−0.0348**	−0.0176	−0.2588***
	(0.0026)	(0.0161)	(0.0108)	(0.0496)
disaster_{t-1}	−0.0108***	−0.0305*	0.0221**	−0.4732***
	(0.0026)	(0.0160)	(0.0107)	(0.0487)
$W \cdot \text{disaster}_t$	0.0008	0.0062**	−0.0024	0.0455***
	(0.0005)	(0.0032)	(0.0022)	(0.0081)
$W \cdot \text{disaster}_{t-1}$	0.0020***	−0.0042	0.0057***	−0.0196**
	(0.0005)	(0.0031)	(0.0022)	(0.0080)
$\ln(\text{pop}_t)$	0.0149***	0.0160***	0.0186***	0.0146***
	(0.0026)	(0.0027)	(0.0027)	(0.0026)
$W \cdot \ln(\text{pop}_t)$	0.0101***	0.0113***	0.0116***	0.0102***
	(0.0011)	(0.0011)	(0.0012)	(0.0011)
$\ln(\text{lights}_{t-1})$	−0.4306***	−0.4318***	−0.4332***	−0.4311***
	(0.0022)	(0.0022)	(0.0022)	(0.0022)
ρ	0.0797***	0.0797***	0.0828***	0.0796***
	(0.0001)	(0.0001)	(0.0002)	(0.0001)
Observations	130,242	129,465	125,496	130,053

Note: ***, **, * denote significance at the 1%, 5% and 10% level. All specifications are SDEM and are estimated by Maximum Likelihood. Standard errors in parentheses. Cell and year fixed effects included but not reported. Spatial radius is r=80 km. Yearly disaster intensities reflect time-weighted rolling averages over 12 subsequent monthly observations.

Table A24: Region: Sub-Sahara Africa

Dependent Variable: $\Delta \ln(\text{lights}_t)$

	wind	**precip.**	**drought**	**cold**
Disaster_t	0.0011	−0.0365	0.0102	0.1513**
	(0.0034)	(0.0281)	(0.0183)	(0.0618)
Disaster_{t-1}	−0.0011	0.0200	0.0454***	−0.0437
	(0.0034)	(0.0274)	(0.0175)	(0.0588)
$W \cdot \text{Disaster}_t$	−0.0003	0.0134*	−0.0010	−0.0080
	(0.0010)	(0.0073)	(0.0052)	(0.0166)
$W \cdot \text{Disaster}_{t-1}$	0.0016*	0.0038	−0.0076	−0.0152
	(0.0010)	(0.0072)	(0.0048)	(0.0158)
$\ln(\text{pop}_t)$	0.0410***	0.0444***	0.0385***	0.0453***
	(0.0094)	(0.0094)	(0.0100)	(0.0094)
$W \cdot \ln(\text{pop}_t)$	−0.0007	−0.0040	−0.0077	−0.0072
	(0.0048)	(0.0047)	(0.0050)	(0.0052)
$\ln(\text{lights}_{t-1})$	−0.4132***	−0.4131***	−0.4180***	−0.4133***
	(0.0044))	(0.0045)	(0.0046)	(0.0044)
ρ	0.0802***	0.0800***	0.0815***	0.0799***
	(0.0014)	(0.0014)	(0.0014)	(0.0014)
Observations	28,140	27,993	26,082	28,035

Note: ***, **, * denote significance at the 1%, 5% and 10% level. All specifications are SDEM and are estimated by Maximum Likelihood. Standard errors in parentheses. Cell and year fixed effects included but not reported. Spatial radius is r=80 km. Yearly disaster intensities reflect time-weighted rolling averages over 12 subsequent monthly observations.